SRNL
SAVANNAH RIVER NATIONAL LABORATORY

ENGINEERED EQUIPMENT AND SYSTEMS

Traditional and Digital Autoradiography Techniques: A Comparison Study

K. M. Gibbs and C. S. Kestin

Publication Date: August 29, 2006

Savannah River National Laboratory
Washington Savannah River Company
Savannah River Site
Aiken, South Carolina

DISCLAIMER

Traditional and Digital Autoradiography Techniques: A Comparison Study

CONTENTS

LIST OF FIGURES

LIST OF TABLES

Traditional and Digital Autoradiography Technique: A Comparison Study

Executive Summary

This report fulfills the FY 2006 Enhanced Surveillance Campaign Level 3 milestones for Task TSR 11.1 as defined in the execution plan [1, 2]. The purpose of this task is to reduce the cycle time necessary to complete analytical evaluations required for surveillance of reservoirs. The development of the digital autoradiography system supports this task. The digital autoradiography system is currently operational and ready for implementation in reservoir surveillance performed in the Materials Test Facility (MTF) at Savannah River Site (SRS). SRS requests design agency (Los Alamos National Laboratory and Sandia National Laboratory) concurrence for the implementation of this system and on the establishment, in conjunction with the Savannah River National Laboratory (SRNL), of the implementation requirements for this system.

Introduction

Stainless steel tritium reservoirs and pinch welded tubes, which have been exposed to tritium for a prolonged period, are destructively evaluated at the end of their service lives for a variety of reasons. One requirement of this evaluation is to assess the tritium diffusion into the reservoir material. The current method used to determine the geometry and depth of tritium penetration is autoradiography. This technique employs a photographic emulsion and has been effective for a number of years. The primary disadvantage of this technique is the time required to obtain results. The success of the traditional technique is dependent on many variables, such as the proficiency of the operators in conducting sample preparation, the geometry of the sample and the shelf life of the photographic chemicals. If results are not satisfactory, several repetitions are often required and usually add weeks to the total analysis time for the sample. Due to the extensive time required for the liquid emulsion autoradiography method, a new, faster technique was desired. Personnel from the Savannah River National Laboratory (SRNL) have been working on a system based on digital imaging technology to replace the current method. The purpose of this report is to provide a description of the current method, a description of the equipment for the new digital method and its capabilities, and a direct comparison of the results between the existing and proposed techniques. The advantages of the digital method is the reduced time of exposure (from 24 hours to around 10 minutes), increased sample throughput, reduced rework of samples, and the elimination of chemical processing.

Traditional Autoradiography Technique

The first step in both techniques requires the destructive removal of one or more samples from various locations of the reservoir. Pieces cut from the reservoir are then prepared as metallographic mounts. The metallographic mounts are prepared in 1.25” or 2” diameter sizes depending on the type of sample. This consists of mounting a metal sample in either bakelite or acrylic media. This mount is then ground, polished, and etched with an

appropriate etchant to reveal the sample's microstructure. Autoradiography is just one of many tests performed on these samples.

The autoradiographic process currently used in reservoir surveillance to determine tritium penetration is a liquid photographic emulsion (photo-emulsion) technique. SRS personnel were trained to use this technique by Mound personnel as part of a technical information transfer. Under darkroom conditions, the sample is coated with the liquid photo-emulsion (KODAK NTB™). The emulsion is heated to ~43^{o}C and rolled onto the sample surface using a glass stirring rod. The sample is typically rolled from areas of low anticipated tritium concentration to areas of high tritium concentration. This process has the potential of transferring tritium from one part of the sample to another, if not performed correctly.

The sample mount is then placed into a light-tight box and refrigerated for 24 hours during which time the liquid emulsion cures and is exposed to the tritium beta and associated low energy x-rays. The emulsion is then developed with KODAK DEKTOL developer and KODAK fixer in situ on the sample, again under darkroom conditions. Silver grains in the emulsion are developed due to the exposure to the beta radiation present in the sample. The location and quantity of silver grains exposed are a function of the location and quantity of tritium present in the sample. The unexposed emulsion is transparent but areas of the photo-emulsion that are exposed to the tritium radiation are transformed to an opaque gray color. This change in the photo-emulsion then provides an indication of the location of tritium in the underlying base metal. Typical results are shown in Figure 1, where the dark gray color indicates the location of tritium. The developed emulsion on the sample is viewed with optical microscopes and the depth of tritium penetration is determined by measuring from the inside surface of the reservoir component (i.e., where the tritium is located during service) to the edge of the "gray contrast zone" (i.e., to where this zone becomes "clear").

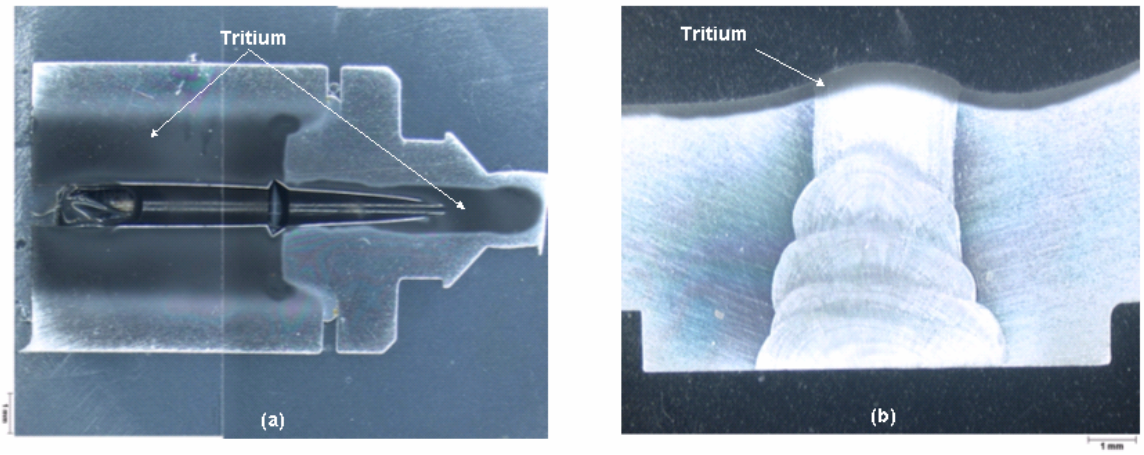

Figure 1: Typical traditional autoradiography results. Reclamation weld (a) and girth weld (b).

The concentration of tritium appears constant except at the very edges where there is an apparent grayscale density gradient. In fact, the concentration of tritium is not constant and the uniform appearance is due to saturation of the photographic emulsion. Saturation is best explained within the context of the exposure/density curve for film, an example of which is shown in Figure 2.

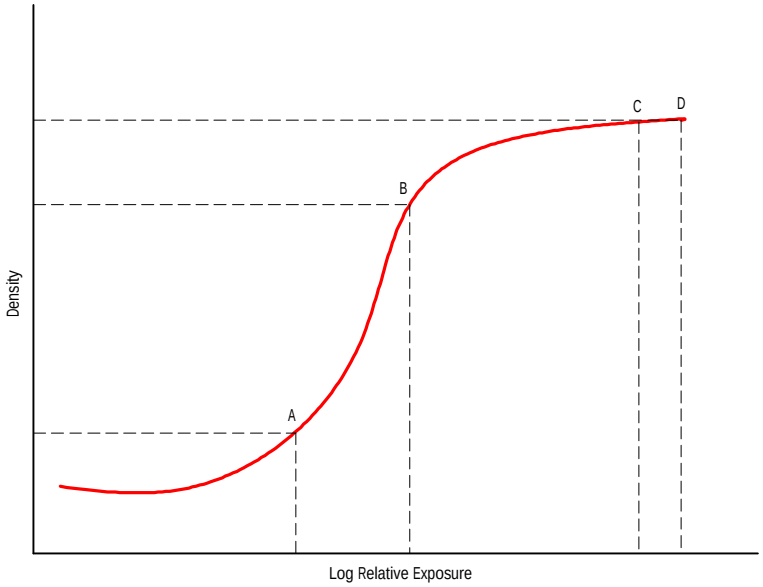

Figure 2: Typical characteristic (exposure/density) curve for film.

In the region of the curve between A and B the photographic density is roughly linearly proportional to the log of the exposure. However, there is virtually no change in density for an increase in exposure between C and D. In this region the film is saturated. The autoradiography process is conducted in the saturation region due to the long exposure time and thus information regarding the gradient of tritium concentration is largely lost.

It has been observed on some samples, as is illustrated in Figure 3, that the emulsion can be developed on the mount material where there is no tritium containing metal, which indicates that tritium contamination can be transferred over the sample surface. Therefore, in some cases tritium can be transferred to regions of the sample that do not have permeated tritium. Improper emulsion application and/or sample geometry can result in this phenomenon.

The major disadvantage of this technique is that the lengthy exposure time and chemical processing requirements. In addition, imperfections in sample preparation, such as gaps between the sample and the mounting compound, require substantial rework and can result in extensive time delays.

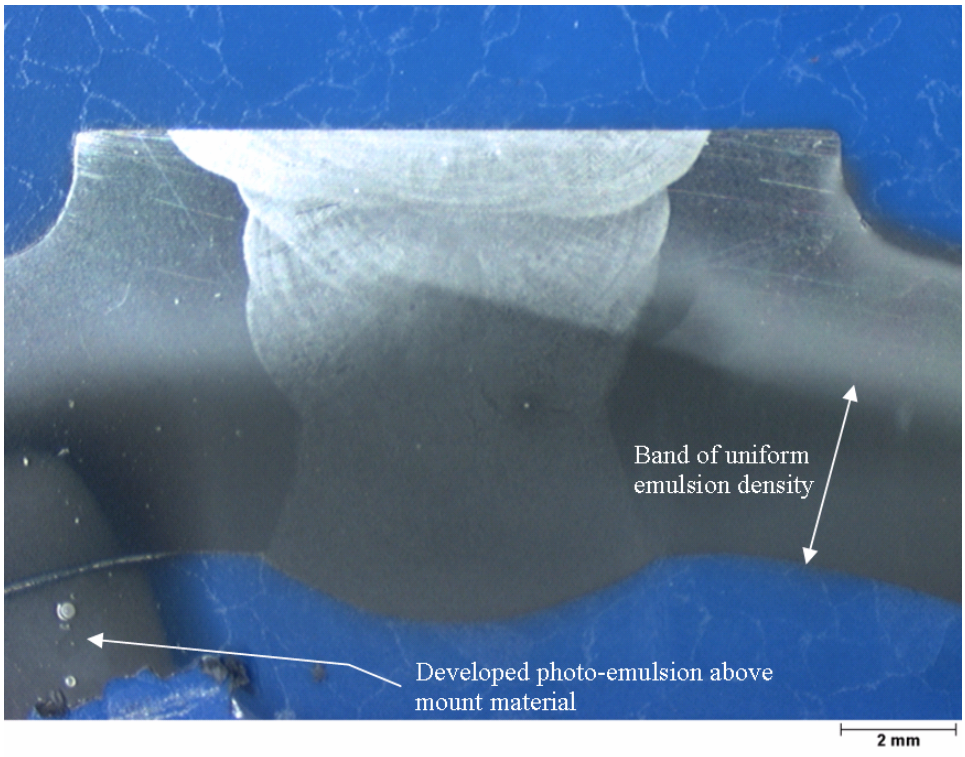

Figure 3: Sample with developed photo-emulsion on the mount material which indicates that tritium contamination can be spread on the surface of the sample.

Digital Autoradiography System Description and Evolution

In October of 2003, SRNL personnel were approached to assist the Materials Test Facility (MTF) personnel with the development of an alternative method to the traditional autoradiography technique. It was found that there were several commercially available systems for autoradiography, but these systems were designed for biological specimens, and none were readily adaptable to the present application. Consequently, it was decided to design and fabricate a custom digital imaging system explicitly for this application.

The proposed solution was an imaging system based on a lens-coupled CCD (charge coupled device) camera. The first step in the system design process was to assess whether the proposed solution was feasible. Due to the contamination issues related to working with tritium, it was desired to demonstrate feasibility with another isotope, preferably a sealed check source. It was determined that a 0.1 μCi Strontium-90 (Sr-90) source would produce as much visible light in the scintillator as the expected average tritium concentration (about 90 appm) in stainless steel. The Sr-90 source was available at SRS in a sealed source configuration and was used with an existing CCD camera to demonstrate the feasibility of the approach. The initial feasibility tests indicated that integration times on the order of minutes would be needed given the field-of-view (numerical aperture) and the anticipated low light levels. The relatively long integration time necessitated the use of a cooled CCD camera to minimize dark current and the associated dark current noise. Based on this information, the system described below

was fabricated and assembled. Figure 4 shows the basic setup for the feasibility study. The visible image of the Sr-90 split source is shown in (a). In (b) a thin (4 mil) scintillator is placed on top of the sample and an image was collected under dark conditions. The image obtained in the dark was superimposed on the visible image in (c).

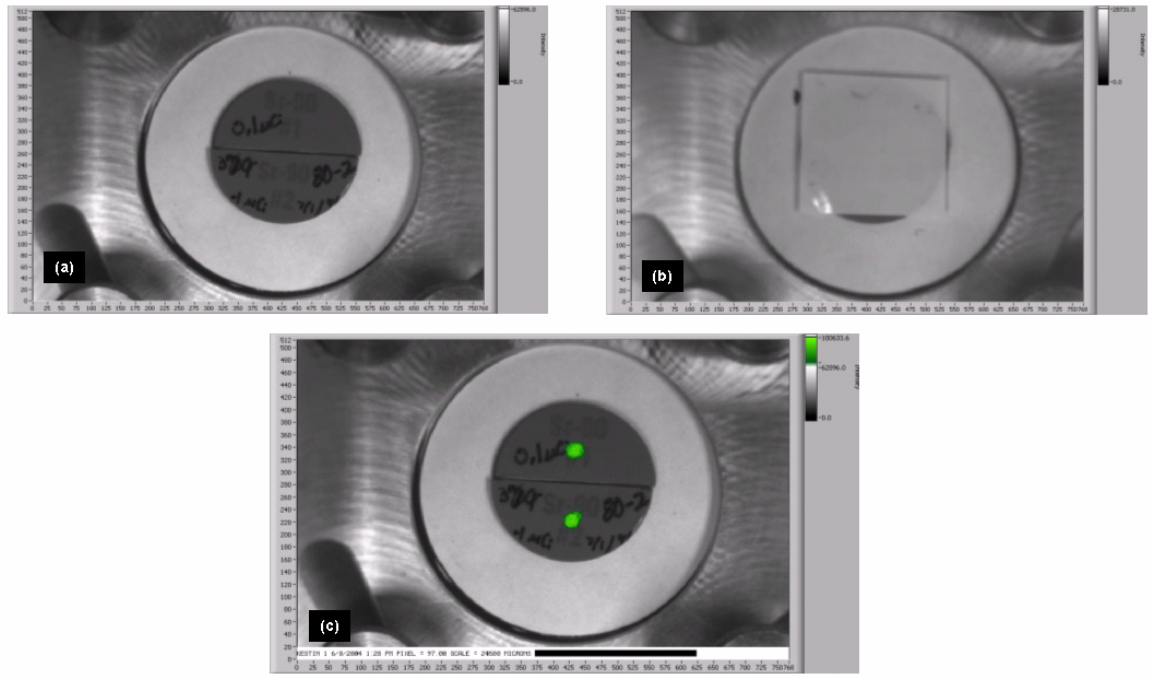

Figure 4: Results from feasibility study with 0.1 *u*Ci Sr-90 beta source. Visible image of split source in (a), image of source and scintillator (b), and composite image (c) showing beta source location.

The prototype system design is shown in Figure 5. The primary components of the system were a cooled CCD camera (Apogee Ulta), lens (Nikon 60 mm f/2.8 Micro), an expandable light-tight bellows, and sample holder and manipulator. The system provided the ability to change the magnification or field-of-view (FOV) by changing the working distance using the vertically oriented linear translation stage. The sample holder is shown in greater detail in Figure 6. The sample is placed on a self-leveling vise to ensure the mount is on a parallel plane with the camera. The vise is tightened so that the sample is pressed to the bottom of the top plate preventing sample movement during the inspection. A phosphor scintillator is placed on top of the sample through the opening in the holder top plate. The scintillator converts the tritium beta and x-ray energy into visible light which is collected by the optical system. The chosen scintillator (BioMax™ Transcreen LE) is manufactured by Kodak and is optimized for low energy beta emitters. It is typically used as an intensifying screen in film-based autoradiography of biological specimens. A glass cover is placed on the scintillator so that the scintillator is held in intimate contact with the sample. Initially, clamps were provided to hold the glass down. Later it was determined that the weight of the glass cover was sufficient to hold the

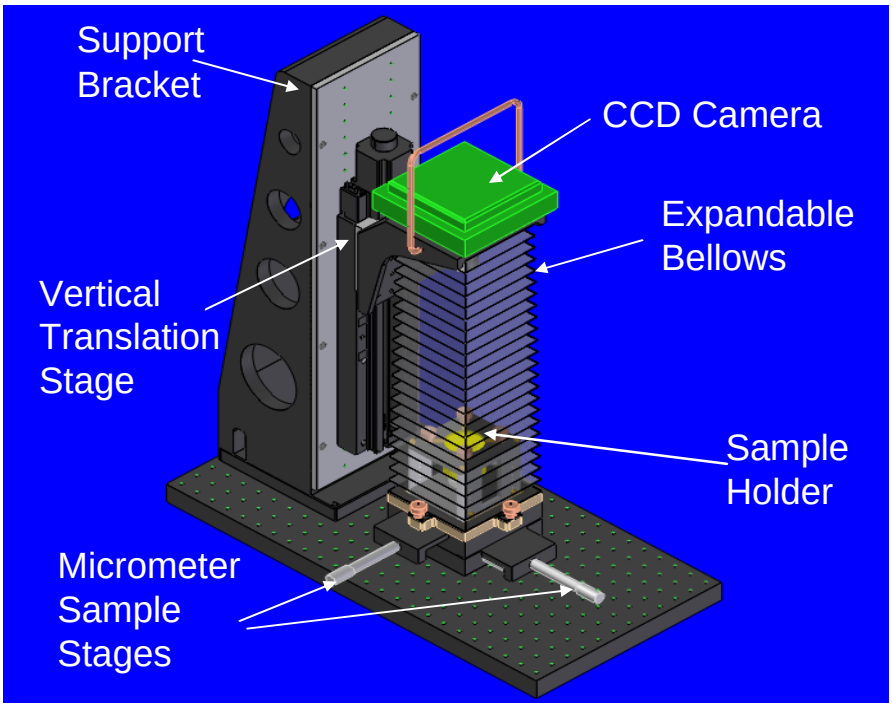

Figure 5: Prototype digital AutoRad system.

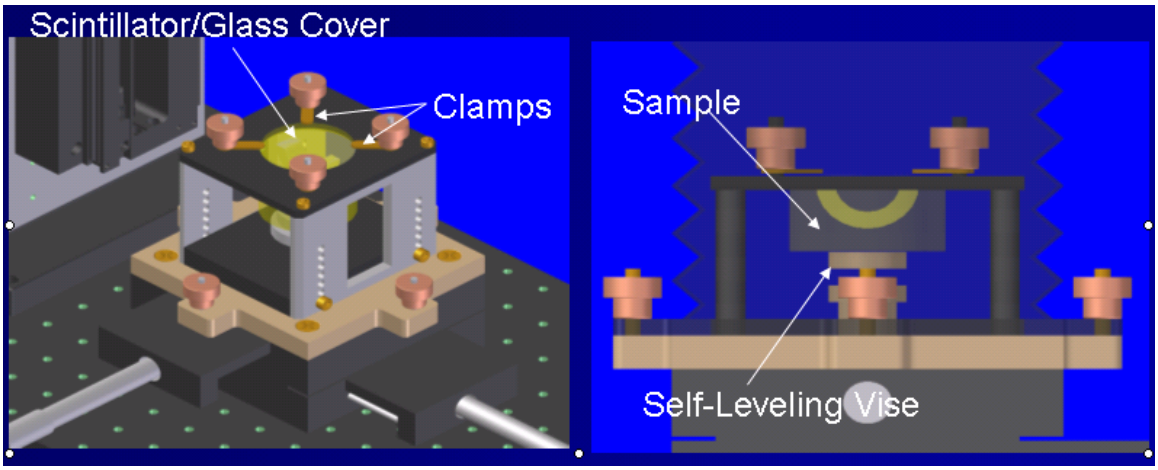

Figure 6: Sample holder details.

scintillator down and the clamps were not needed. The 2-axis manipulator is used to move the sample within the system FOV.

Typical results obtained in FY 04, using the prototype digital AutoRad equipment, are shown in Figure 7. These images were obtained in 5 to 10 minutes with the digital system, rather than 1 to 2 days as required with the traditional photo-emulsion based method. For comparison, the traditional autoradiography images are shown in Figure 8. The location of tritium is indicated by the green color superimposed on the visible images. The irregular or "blocky" edges are due to the high dark current noise level of the CCD camera and the statistical based image processing performed to differentiate

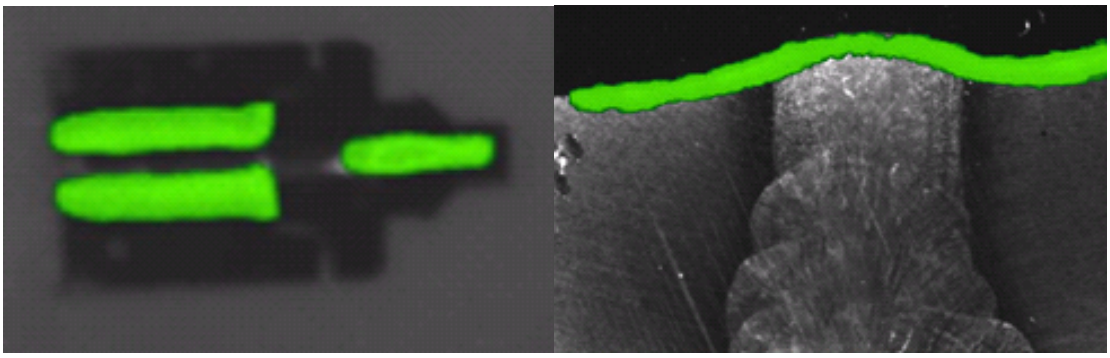

Figure 7: Typical results with prototype system and 5 to 10 minutes exposure.

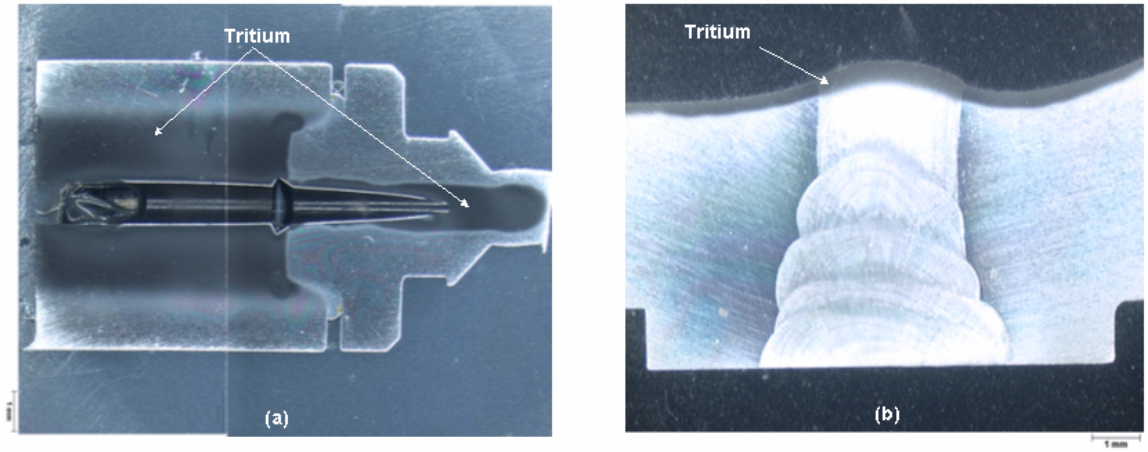

Figure 8: Traditional autoradiography results on the same samples as in Figure 7.

signal and noise. A detailed description of this processing will be provided later in the report.

It was determined that the results could be substantially improved using a higher quality camera. In FY 05, a new camera (Photometrics Versarray 1024 x 1024 CCD Camera) was purchased. The new camera has significantly less dark current noise due to thermoelectric cooling to -70 °C rather than to -20 °C as in the case of the prototype CCD camera (Apogee Ulta). At this temperature the dark current and associated noise is extremely low and the system noise is dominated by the readout noise. This noise level is minimized by using the slowest readout speed and lowest gain settings on the camera. In addition to the camera upgrade, the mechanical design was modified to incorporate the new camera and to enhance the ergonomics of the sample holder and bellows interface.

The interface details of the light-tight bellows, which must be removed for sample placement and camera focus adjustments, were improved to facilitate rapid attachment and detachment while ensuring a light-tight connection. The camera interface software and image analysis software were modified to accommodate the new camera. The upgraded system is shown in Figure 9.

The ergonomic changes were primarily in the design of the sample holder to make it easier for an operator wearing rubber gloves to fixture the samples. The sample table was added to allow for larger variation in sample height since the self-leveling vise has only a 0.5 inch travel range. A centering cup was added to hold and center the sample and is attached to the self-leveling vise, which is not shown in Figure 9. The operator can switch between sample sizes (1.25 and 2 inch) simply by changing the top plate using the three screws shown.

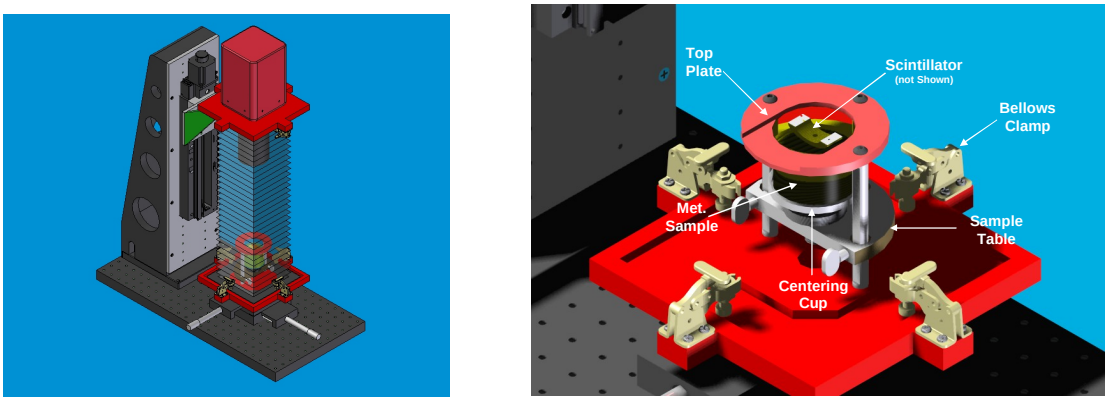

Figure 9: Modified digital AutoRad system design (left) and the details of the new sample holder (right).

After completing the upgrades, several autoradiography samples were examined to test the performance of the system. Typical sample results are shown in Figure 10. The results from the lower noise camera are clearly superior to the results from the prototype system in terms of eliminating the "blocky edges". In addition, variations in tritium concentration are readily observable, which was not the case with the original camera. These images were obtained in the 5 to 10 minute range.

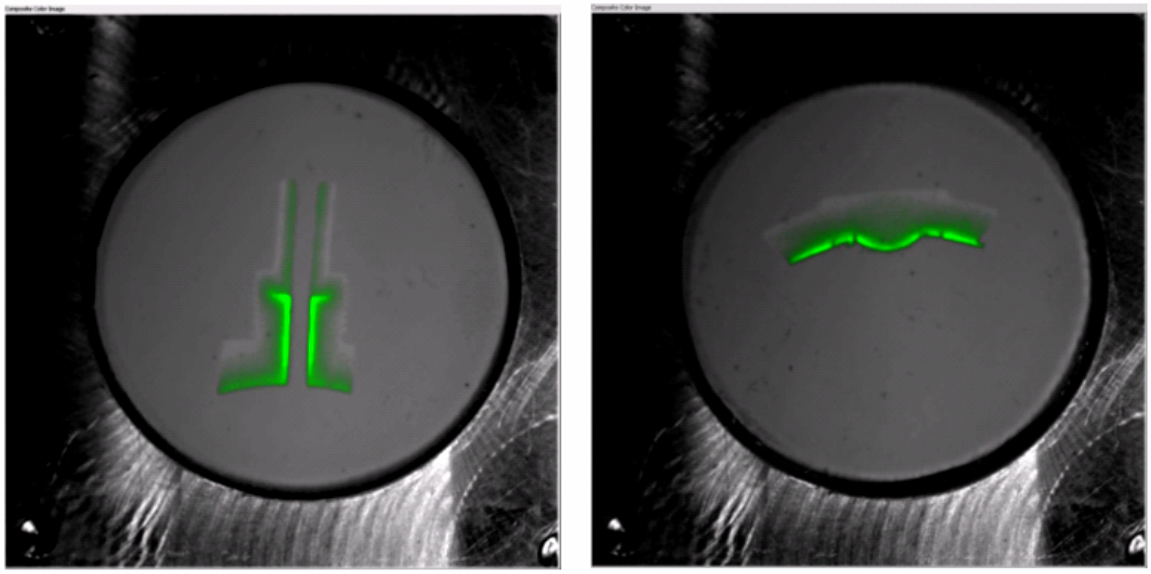

Figure 10: Digital AutoRad images acquired with new low noise camera.

Dimensional calibration of the digital AutoRad system was needed to provide accurate quantitative measurement of tritium penetration. The calibration involved relating the vertical stage position (related to the camera-to-sample distance) to the CCD image field-of-view or pixel size. First, a rough correlation between FOV and stage position was performed. Then the system was calibrated at several FOV's using images of precision ground stainless steel gage blocks as shown in Figure 11. The blocks were retained in a slotted plastic holder made to fit in the digital AutoRad sample holder.

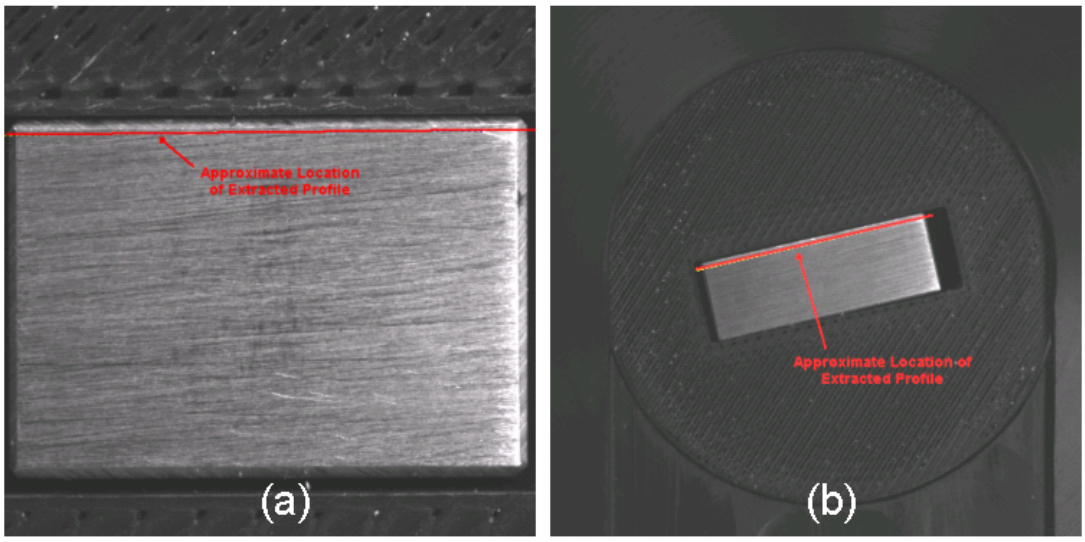

Figure 11: Gage blocks for calibration at 13 mm FOV (a) and 60 mm FOV (b).

A line profile, parallel to the edge of the gage block as shown in Figure 11, is extracted from the image. The derivative of the line profile, shown in Figure 12, has two prominent peaks located at each end of the profile which represent the edges of the gage block. The peaks at the ends of the profile actually have dual peaks which are due to the chamfer on the edges of the gage block. The extreme most peaks are then used to establish the gage block length in pixels. The physical length of the gage block divided by the length in pixels yields the pixel size at that particular FOV. The largest error in calibration occurs at the largest FOV (60 mm). At the 60 mm FOV the accuracy is estimated to be +/- 0.22% of the calculated pixel size. This method was performed for 13, 15, 18, 20, 25, 30, 35, 40, 45, 50, 55, and 60 mm FOVs. These results were then used to create the calibration curve of stage position versus pixel size provided in Figure 13 and are the basis for the *Select FOV* subroutine shown in Figure 17, which will covered in the software description section of the report. The stage positions were obtained using the rotary encoder readings from the stage. The accuracy on stage position is driven primarily by the accuracy and repeatability of the lead screw which is +/- 0.04 mm. The effect of this error is a maximum where the slope of the calibration curve is largest and is estimated as +/- 0.12% of the calculated pixel size. The overall accuracy of the calibration is the sum of the two sources of error which would be +/-0.34%. The system FOV is simply the number of rows or columns of the CCD imager (1024 x 1024) multiplied by the pixel size.

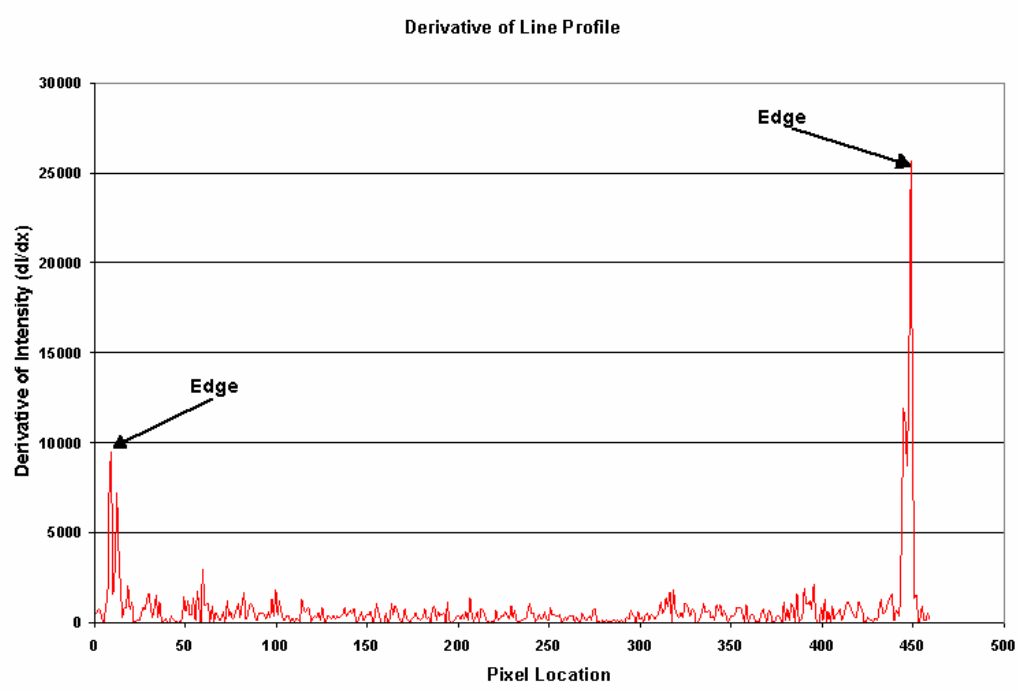

Figure 12: Derivative of gage block line profile.

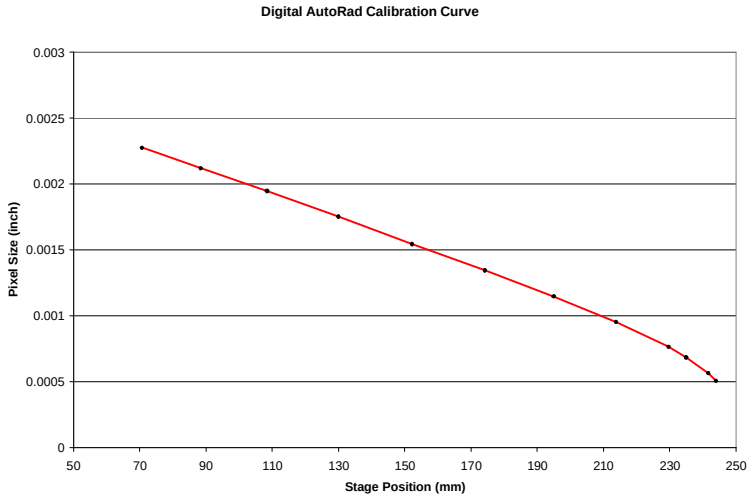

Figure 13: Dimensional calibration curve for the digital AutoRad system.

Digital Autoradiography Technique

The digital autoradiography method can be described as follows. A metallurgical mount is loaded into the sample holder with the glass cover plate and a visible image is obtained (with the bellows removed from the system). Next, the scintillator sheet is placed in direct contact with the sample surface, between the sample and the glass cover plate. The bellows assembly is installed to provide a light-tight environment. The tritium image is then acquired, with typical integration times ranging from 5 to 10 minutes. The software

processes the raw tritium image, and then merges the gray-scale visible image with the processed tritium image. This composite image displays the acquired tritium data in shades of green. This presentation clearly differentiates the visible and tritium information. Representative images are provided in Figure 14.

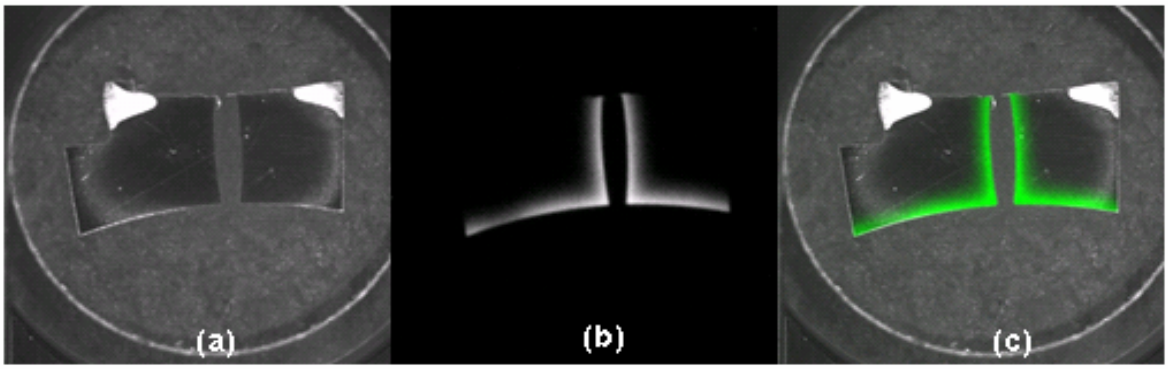

Figure 14: Digital autoradiography images of a reservoir component: (a) visible image; (b) tritium image; (c) composite image.

Digital Autoradiography System Software

The system software consists of two major modules, the data acquisition module and the image measurement and analysis module. These modules are custom designed software created using the LabVIEW ™ programming language. LabVIEW ™ is a graphical programming language where each program has a "front panel" that serves as the user interface and an underlying "wiring diagram" where data flow and processing are mapped.

Data Acquisition Module

The front panel for the data acquisition module, *AutoRad06 Shell*, is shown in Figure 15. A typical underlying wiring diagram is shown Figure 16. When the user runs the *AutoRad06 Shell*, the program prompts the user to enter a sample identification number. The vertical stage is automatically moved to the "home" position to ensure that the stage is placed in a known state. Next the user selects the desired system FOV or pixel size based on the size of the sample by pressing the "Select FOV" button on the front panel. The user has a choice of discrete FOV settings (13, 18, 25, or 35 mm) or a user defined FOV over the range of 13 mm to 60 mm. The 13 mm setting is the limit of the lens and the 60 mm setting is the largest value included in the calibration since the largest samples are 50 mm (2-inches). The calibration curve is used to determine the stage position for the desired FOV or pixel size in the *Select FOV* window, shown in Figure 17. This window shows that the nominal 35 mm FOV (34.93 mm) has been selected. This relates to a pixel size of 0.0341 mm (0.001343 inches) and a stage position of 174.2386 mm. These selections are marked on the calibration curve (red) with a yellow square. Note that the reason mixed (mm and inches) units are reported is because the native unit for the stage control are mm and the desired unit for tritium penetration by the end users are inches.

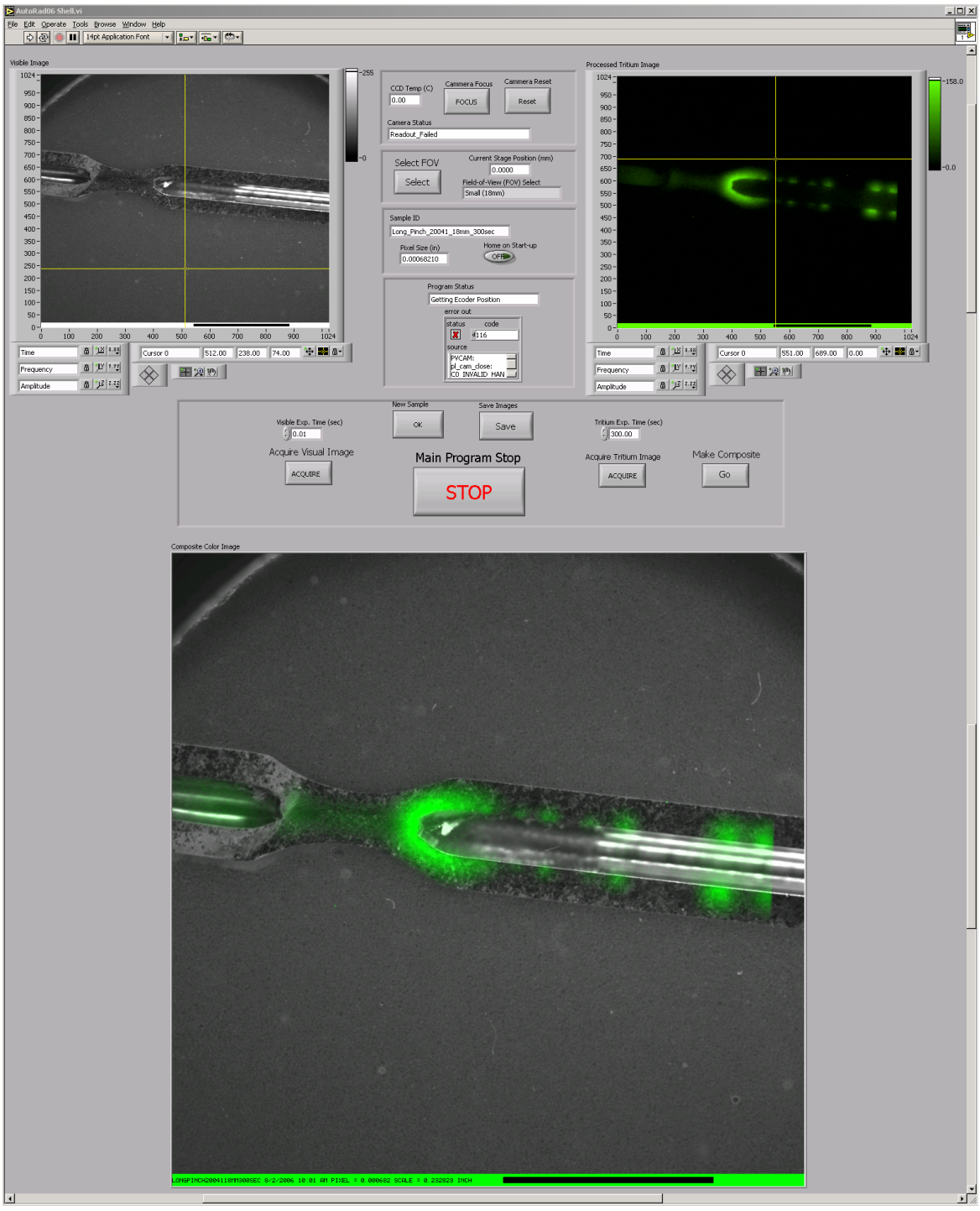

Figure 15: AutoRad06 Shell data acquisition front panel.

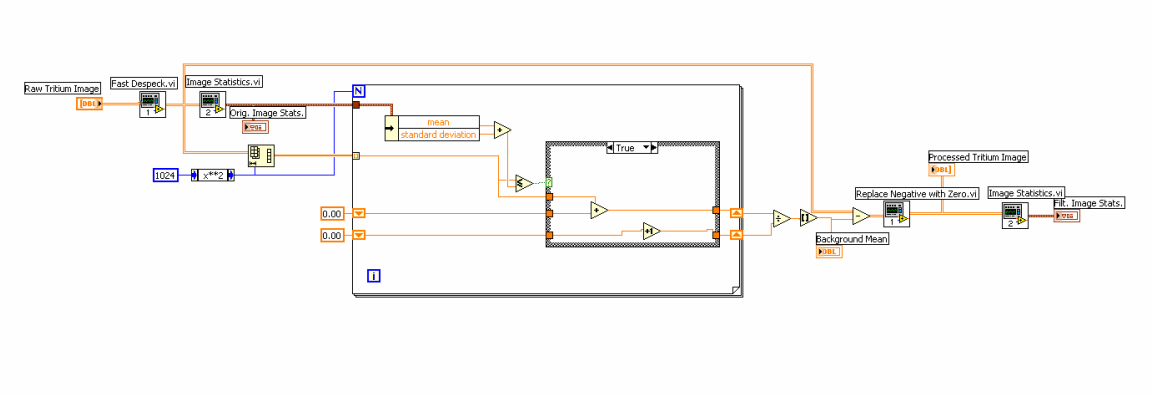

Figure 16: Typical LabVIEW ™ wiring diagram.

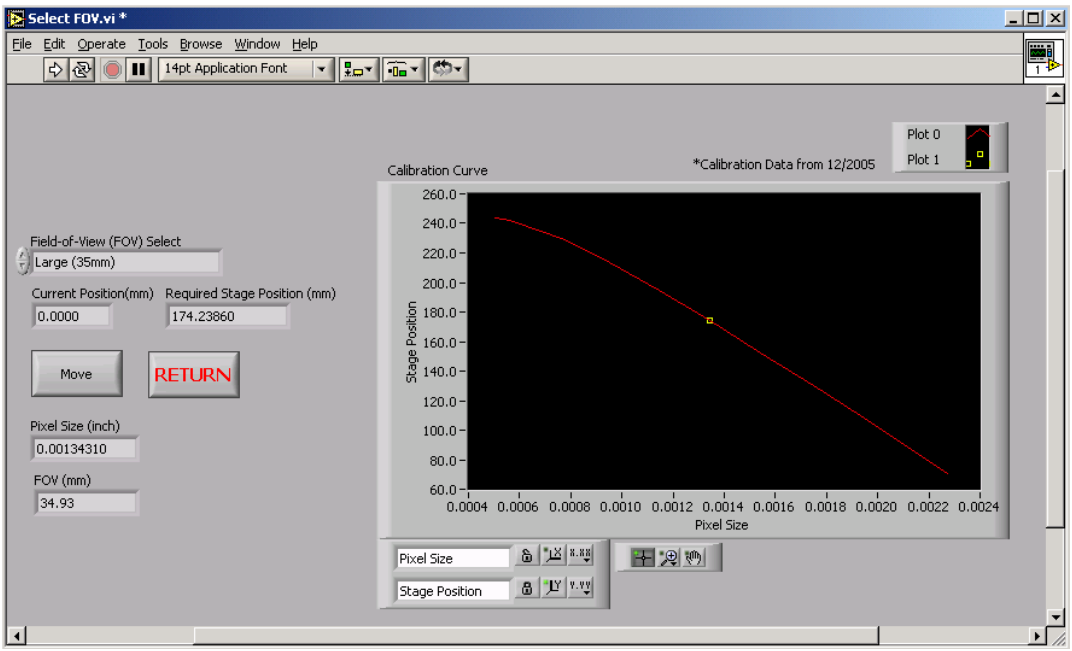

Figure 17: Select FOV window allows users to pick FOV/pixel size.

After selecting the FOV, the software controls the vertical stage motion automatically, then prompts the user to focus the camera's lens. Coarse adjustment marks on the lens allow the user to obtain a reasonable focus quickly and fine tuning is aided by the Focus button, which opens the *Focus* subroutine window. The fine focus adjustment can be done qualitatively using a sample or it can be performed quantitatively using a "focus standard". The focus standard consists of a disk that is half black and half white as shown in Figure 18. An image of this standard is obtained and the center row profile is extracted. The derivative of the center row yields a "gaussian-like" peak and the sharper the peak the better the focus. The sharpness can be quantified by the measuring the "full-width-at-half-maximum" (FWHM). The FWHM is reported as the width value in the Focus window. The user then initiates a focus sequence while adjusting the focus ring.

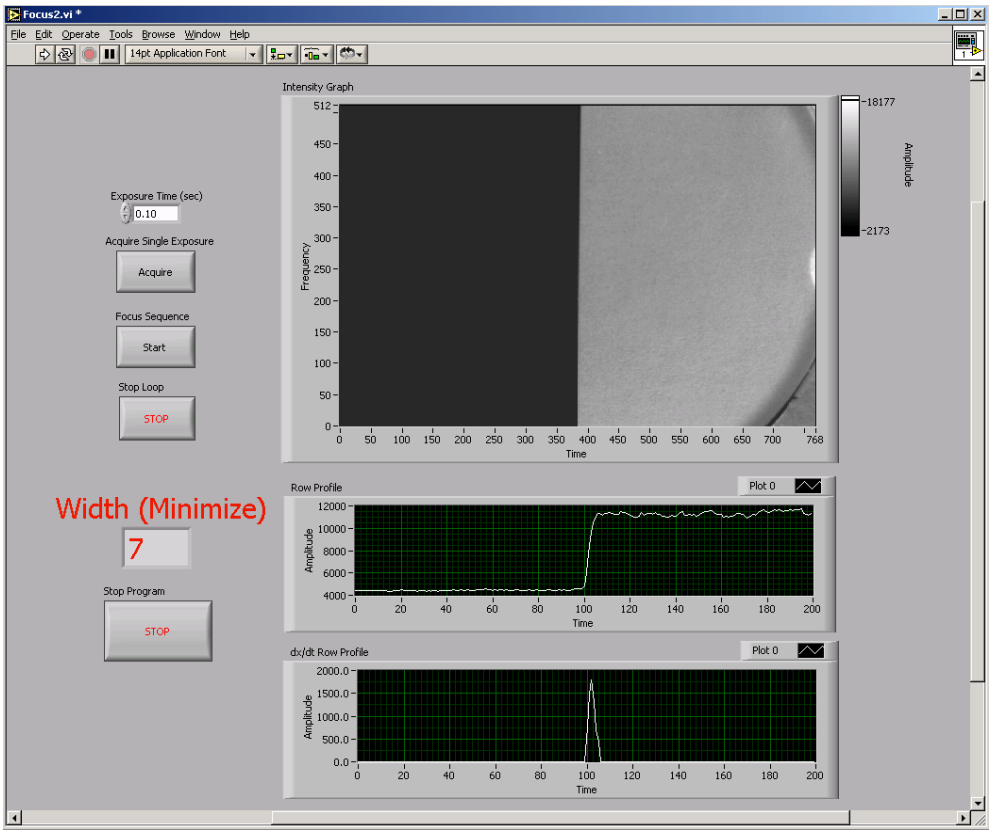

Figure 18: Focus window aids user in focusing the camera.

During the focus sequence the user's goal is to minimize the reported width, which results in the optimal focus. It should be noted that the glass cover plate that holds the scintillator flat should be placed on top of the focus standard because it has a slight effect on the focus.

The *AutoRad Shell* data acquisition module controls the basic camera functions which occur in the background as well as providing the buttons for visual image acquisition and tritium image acquisition. The visual and tritium image each have their specific exposure times that are individually adjustable. Typical visible exposure time is 0.01 seconds and typical tritium exposure time is 300 to 600 seconds. The minimum exposure time is limited by the mechanical shutter to 0.001 second and the maximum exposure time is limited by the camera hardware to 8568 seconds (2.38 hours). Once the images are acquired, the visible image is displayed on the top left of the front panel and the tritium image is displayed on the top right of the front panel. After the tritium image is obtained and processed, the visible and processed tritium images are then merged to form the composite image, displayed at the bottom of the front panel (Figure 15).

The tritium image is automatically processed using the *Process Tritium Image* subroutine which is shown in Figure 19. In Figure 19, the raw tritium image displayed on the left side of the front panel is barely distinguishable from the background. This image is the summation of the CCD camera bias level, the CCD dark current, noise (dark current and

Figure 19: Process Tritium Image window is used to convert the raw data from the camera to an image suitable for making the composite image.

readout), and the desired tritium signal. The unwanted contributions need to be removed from the raw image so that a useful composite image can be created.

The bias level is on the order of about 1000 counts out of an image maximum of 65,535 (16 bit ADC). The tritium signal varies with concentration but is generally 300 counts or less in a 300 second exposure. The dark current and dark current noise at -70 °C is negligible. The readout noise is on the order of +/- 15 counts. Typically, there are also isolated "hot" or bright pixels which are caused by direct hits to the CCD by cosmic radiation over the long integrations. These bright spots are removed using a custom design despecking algorithm which has negligible impact to the rest of the image. The bias level is removed by using statistical processing. The result of despecking and bias removal is shown in the image to the right in Figure 19.

As mentioned earlier, the software automatically merges the visible and tritium images to form the color composite image shown in the bottom of the *AutoRad Shell* front panel shown in Figure 15. The first step in the process to create the composite color image is to normalize the visible and tritium images to 8 bit images (0 to 255) for display only. The normalized images are added such that the visible image contributes equally to the red, green, and blue channels, and the tritium image contributes only to the green channel. The addition of the two images in the green channel can be accomplished by giving the

visible and tritium equal weight (unweighted method) or by assigning a weighted value to the tritium image proportional to the tritium image intensity (weighted method). The advantage of the weighted method is that high intensity values are not saturated or clipped to 255; however, the low intensity values are difficult to see. With the unweighted method the low intensity values are easier to see but the high intensity values are allowed to saturate. Because the primary objective is to measure tritium penetration, the unweighted method was ultimately selected. Figure 20 illustrates the difference in the color composite image using the unweighted method (a) and weighted method (b). The issue of "weighting" only applies to the creation of the composite image, the original tritium image data file is preserved and is used directly for measurement and quantitative analysis.

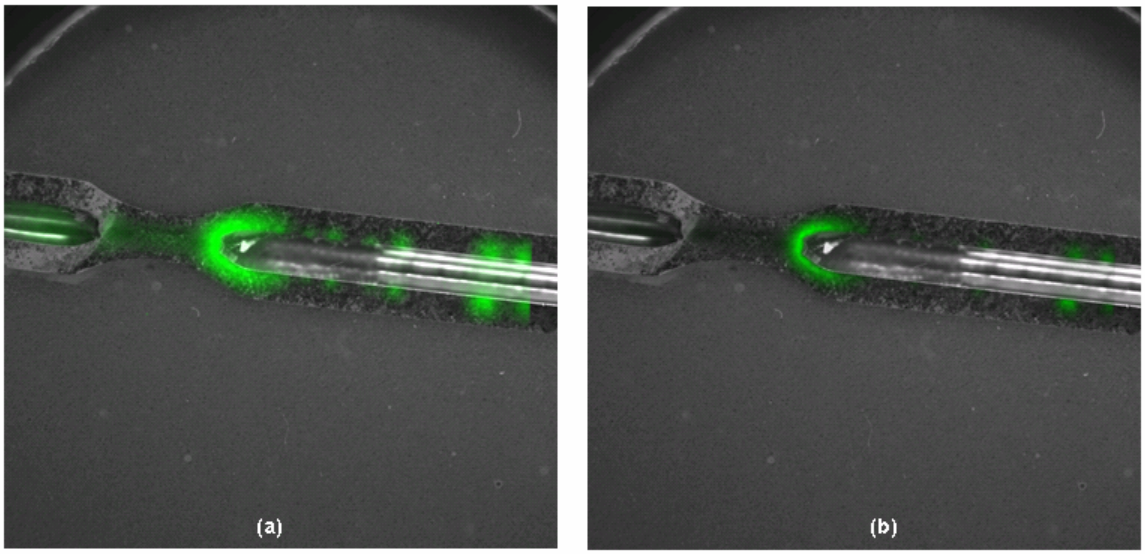

Figure 20: Comparison of color composite images using the unweighted method (a) and the weighted method (b).

Misalignment has been observed occasionally between the visible and tritium images. This is most likely due to bumping the camera during bellows installation creating an offset between the two images. To rectify this issue, the user would obtain another visible image with the bellows removed and press the "Make Composite" button on the *AutoRad Shell* front panel, which allows the user to manually initiate the formation of the color composite image. There is no need to collect another long duration tritium image.

The "Save Image" button on the *AutoRad Shell* front panel, when pressed, saves the visible image and tritium images as raw data files and JPEG files, as well as a color composite image in JPEG format. It also saves an information file with other useful information regarding the inspection. An example of the information file is shown in Figure 21.

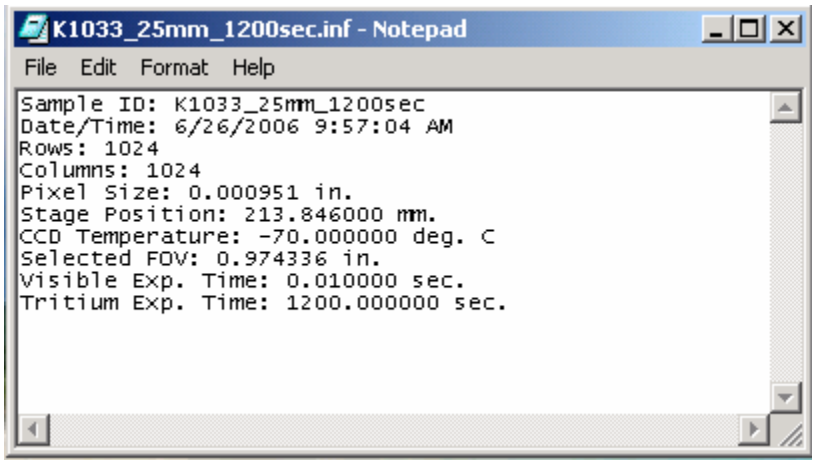

Figure 21: Example of the content of a typical inspection information file.

Image Measurement and Analysis Module

The second portion of the digital AutoRad software is the measurement and analysis module. This module is separate from the data acquisition module and can be run any time following data acquisition. The basic purpose of this software is to assist the user in obtaining unbiased and consistent measurements of tritium penetration.

Figure 22 shows the front panel of the *Main AutoRad Analysis* Shell. When this program is executed the user is prompted to select an image file for analysis and the data is then automatically loaded. The color composite image is displayed on the front panel and the visible and tritium images are also loaded into memory. The user then presses the "Add Profile" button, which allows the user to specify the analysis region as shown in Figure 23. The user defines the end points of the "yellow" line in Figure 23 and the software automatically defines the "red" box and the "blue" perpendicular line. The yellow line is the profile line, the blue line is an alignment aid, and the red box is the region extracted for further analysis. Once the user selects the start point of the yellow line by a mouse click, the software updates the lines and box in real-time as the user moves the mouse. The user selects the profile endpoint by a second mouse click.

After the region is specified, the *Extract Region and Profile* subroutine, shown in Figure 24, is automatically executed. The image subregion data is automatically rotated such that the yellow line is oriented in the vertical direction as shown in the "Visible Image" window of Figure 24. The user then adjusts the two red horizontal cursors in the "Visible Image" window to set the limits for the tritium penetration measurement. These cursors are usually set at the edges of the sample, since there should be no tritium outside the sample. The user then adjusts the "red" vertical cursor in the "Visible Image" window to select the desired column for the tritium profile. The cursors in the "Processed Tritium Image" window automatically follow the movement of the cursors in the "Visible Image" window. When the cursor adjustment is complete, the user presses the "Get Profile" button. This extracts the profile data from the tritium image data as can be seen in the "Intensity Profile" window of Figure 25.

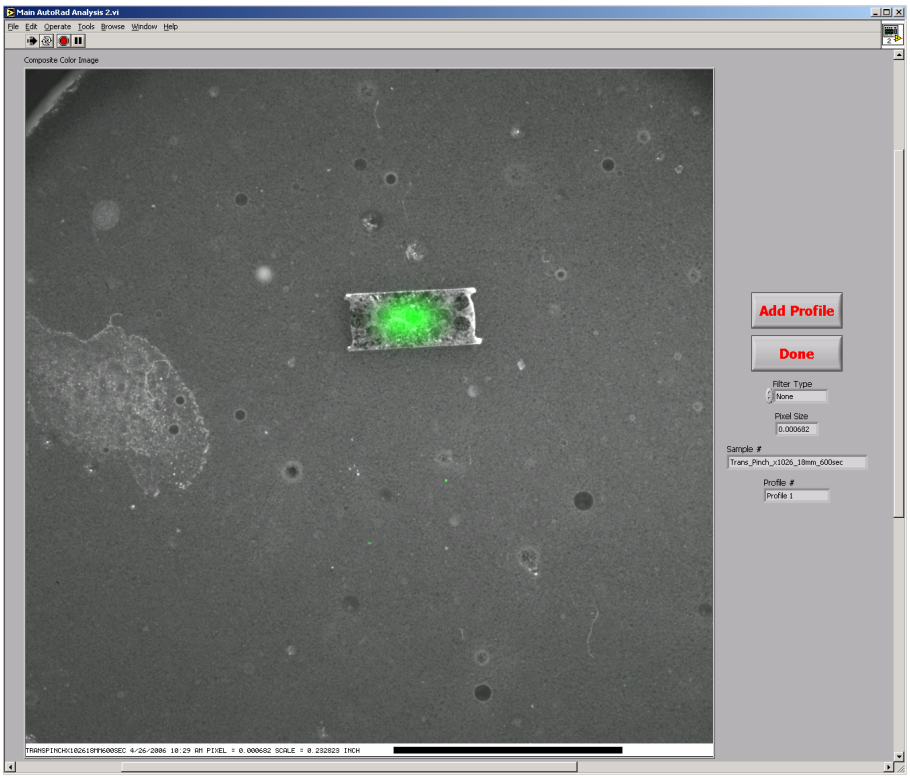

Figure 22: Front panel of the *Main AutoRad Analysis* shell.

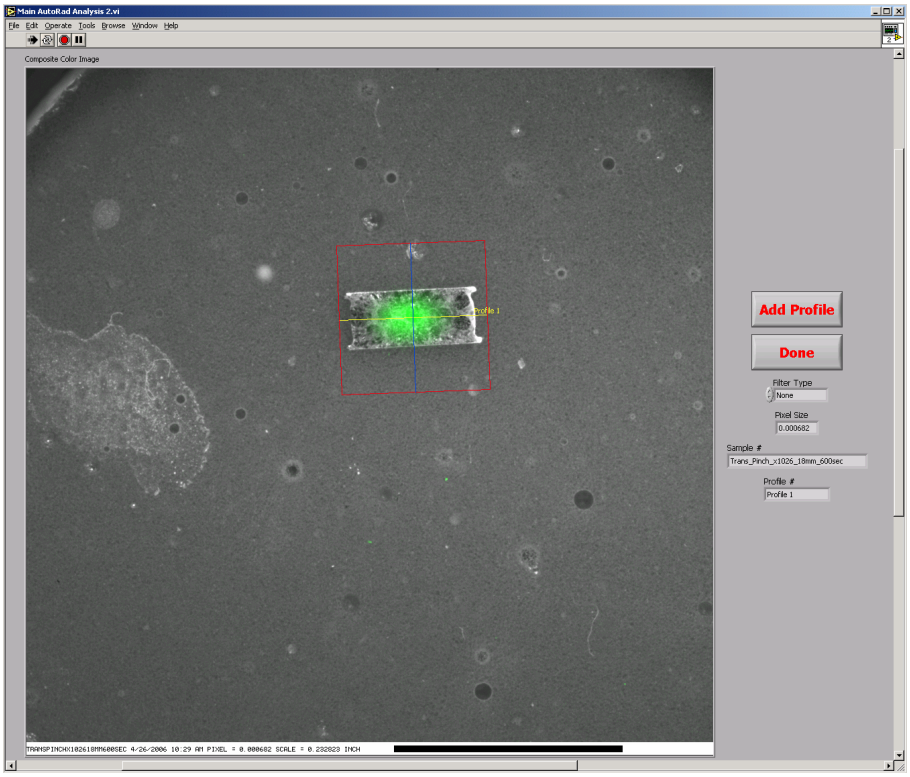

Figure 23: Region and profile line selected for analysis.

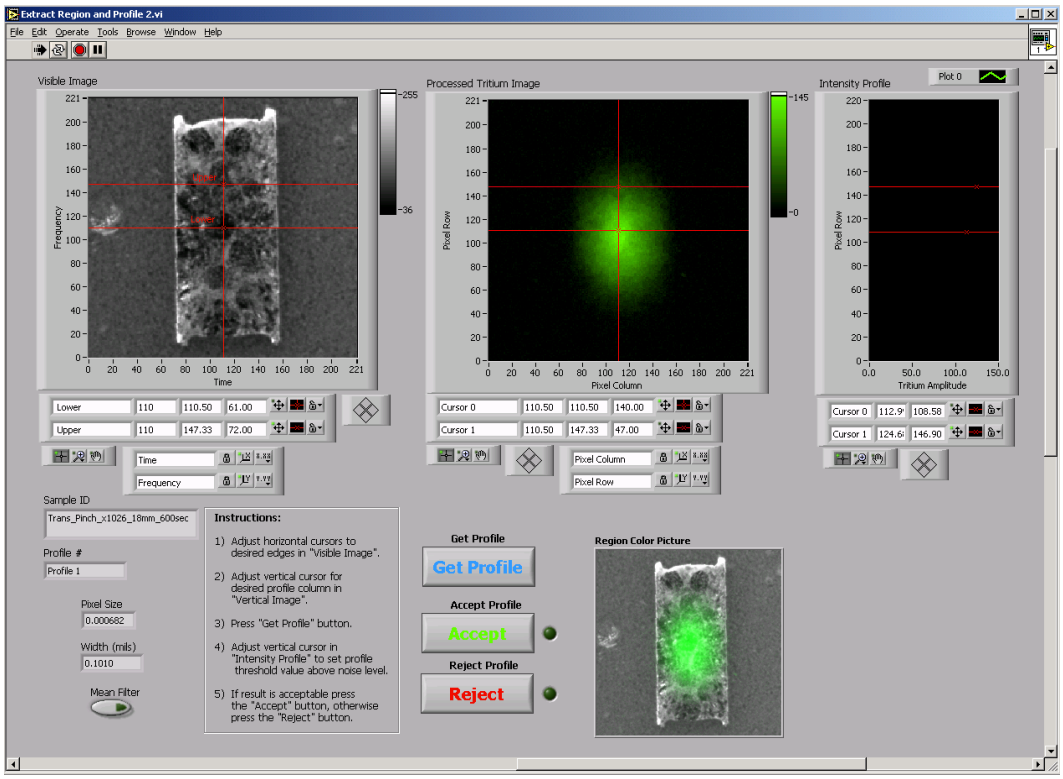

Figure 24: Front panel of the *Extract Region and Profile* subroutine.

At this point, the user can "Accept" or "Reject" the extracted tritium intensity profile. If the "Reject" button is pressed the operation is cancelled and control is passed back to the *Main AutoRad Analysis* Shell. If the "Accept" button is pressed, the *Get Width from Profile* subroutine is executed. The *Get Width from Profile* front panel is shown in Figure 26. The intensity profile is shown in the "Profile Input" window. The data between the red horizontal cursors is extracted and the displayed (rotated 90°) in the "XY Graph 2" window. The data points are fit automatically using a polynomial fitting subroutine. The polynomials fits are shown as solid lines. The penetration widths are measured between the polynomial fits, which reduces the impact of noise on the measurement. The user now adjusts the threshold (horizontal cursor) in the "XY Graph 2" window. As the user adjusts the threshold, the width (or penetration depth) is updated in real-time. In Figure 26, the reported width is shown to be 0.0521 inches when the threshold is set at 54.2122. In Figure 27, the reported width is 0.0981 inches at a threshold of 4.7314. The appropriate setting of the threshold should be set at just above the background noise level as in Figure 27. When the user is satisfied with the threshold setting the "Accept" button is pressed. When this button is pressed, the data is saved as an ASCII data file, for subsequent evaluation, and the "Region Color Picture" in the "Extract Region and Profile 2" subroutine is annotated as shown in Figure 28, and is also saved to file.

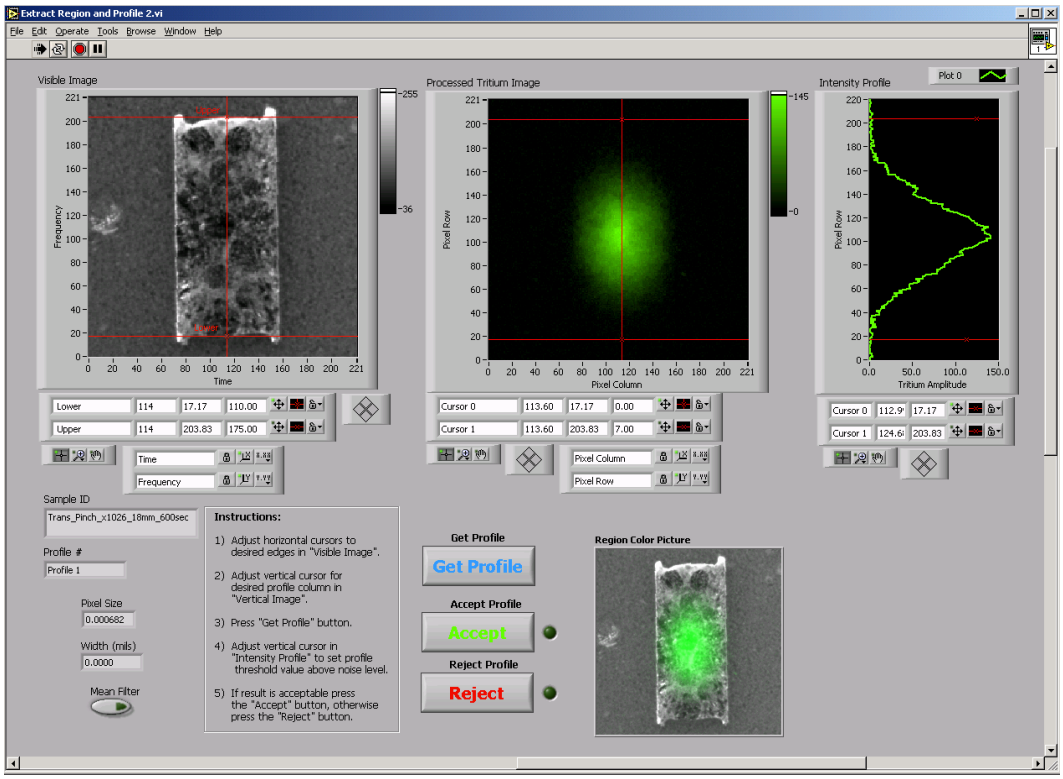

Figure 25: Front panel of the *Extract Region and Profile* subroutine showing upper and lower limits and the extracted profile.

Another feature available in the "Extract Region and Profile2" subroutine is the ability to filter the tritium image to reduce noise. Currently, this filter is a "mean filter" (14 x 14 kernel), which has the effect of smoothing the tritium image and profile and reducing the impact of noise as demonstrated in Figure 29. Using the smoothed data, the threshold level can be lowered to 3.4312 and the width is measured as 0.1010 inches as shown in Figure 30.

Figure 31 compares the results of the measurement using unfiltered and mean filtered tritium data to the traditional results. While both results appear to be in good agreement with the traditional result, care must be taken using the mean filter near discontinuities in the tritium image. The filter will blur sharp edges and can impact the penetration depth measurement. However, if the edge is defined by the unfiltered visible image, then the impact on the penetration measurement will be minimal.

Figure 32 shows a graph created from the archived profile data from the inspection above compared with a "Gaussian" fit. The Gaussian function (Eq. 1) is the solution of the diffusion equation for a point source of tritium. It is interesting to note the agreement between the expected theoretical distribution and the experimentally measured result.

Eq. (1)
$$I = I_0 \exp\left[-\mathrm{p}\left(\frac{x - x_0}{\mathrm{s}}\right)^2\right]$$

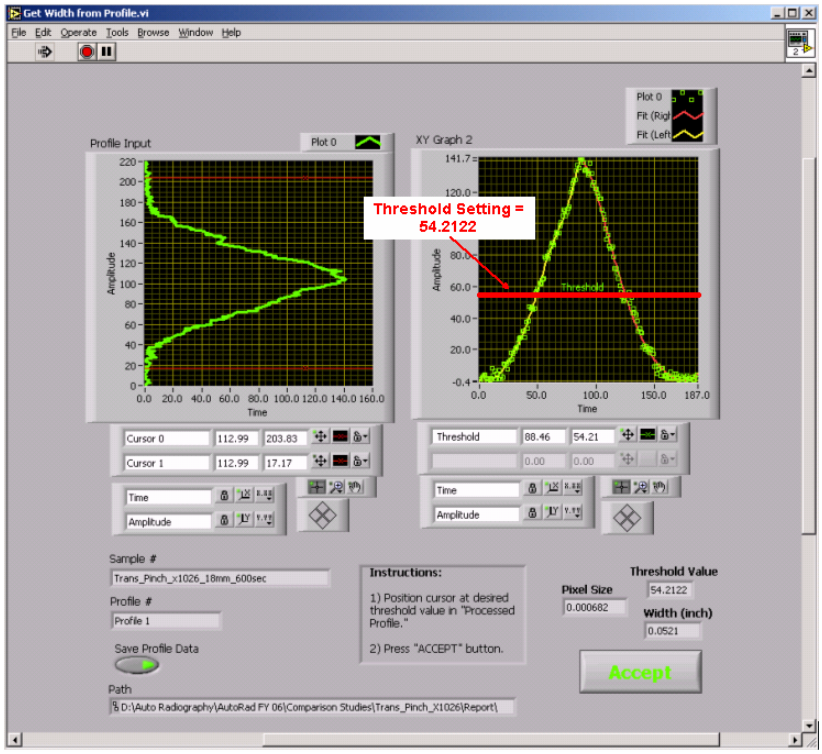

Figure 26: Front panel of the *Get Width from Profile* subroutine showing measured width of 0.0521 inches at a threshold of 54.2122.

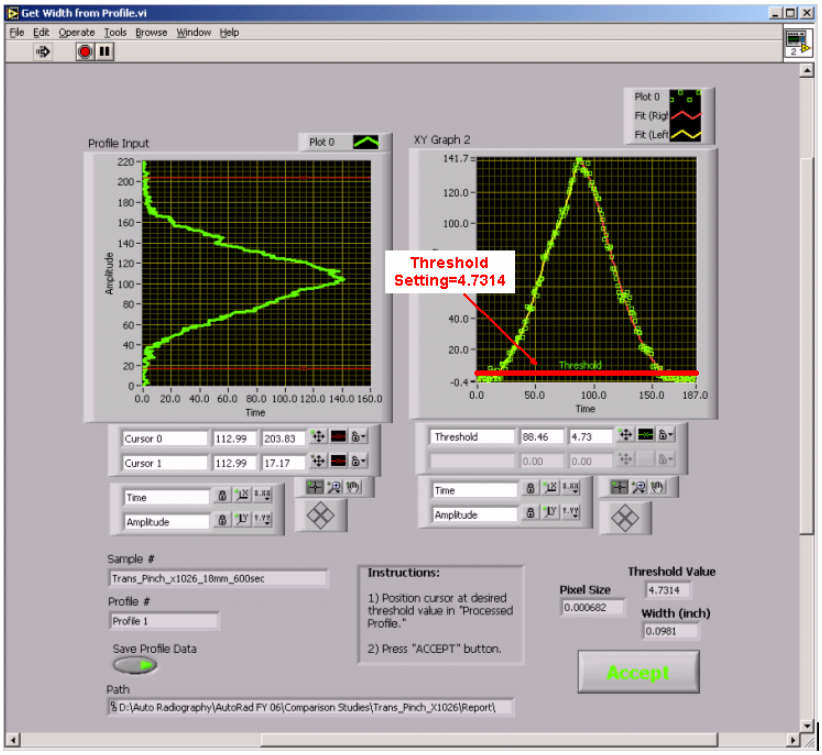

Figure 27: Front panel of the *Get Width from Profile* subroutine showing measured width of 0.0981 inches at a threshold of 4.7314.

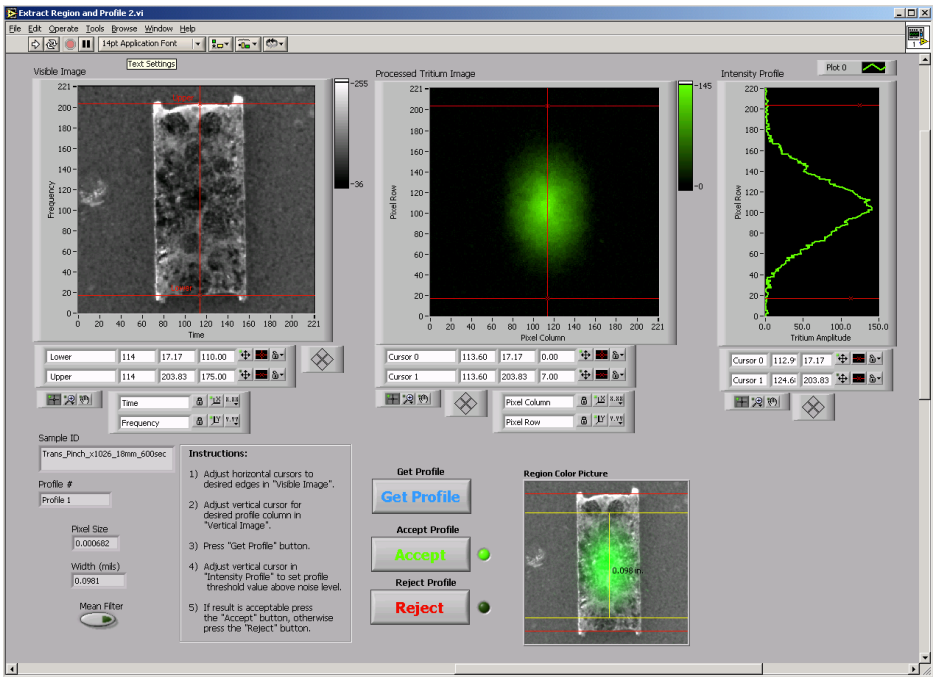

Figure 28: Front panel of the *Extract Region and Profile* subroutine showing measured width obtained from the *Get Width from Profile* subroutine and the annotation of the Region Color Image.

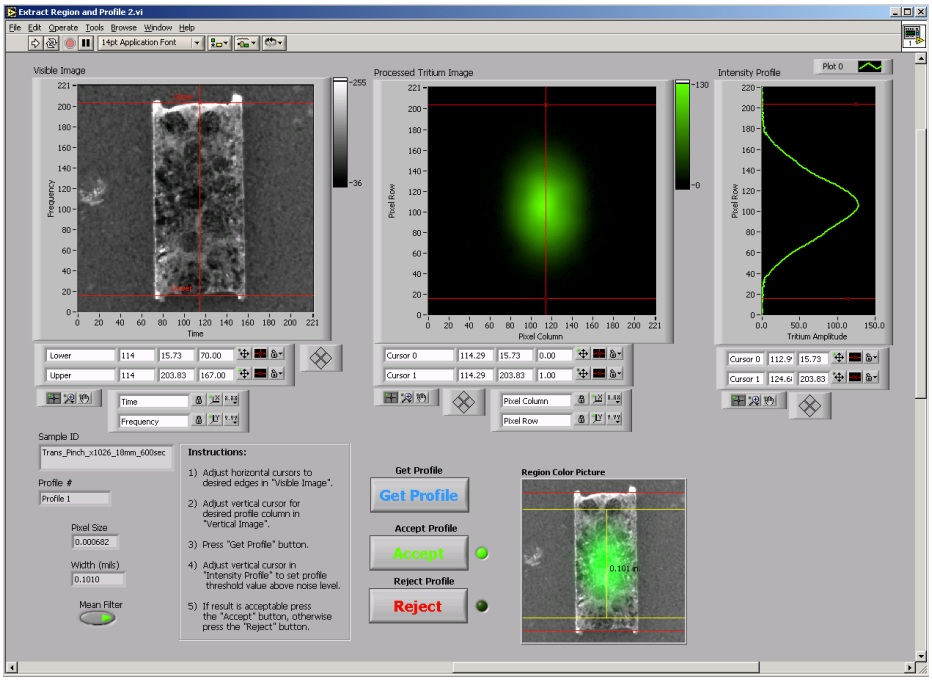

Figure 29: Front panel of the *Extract Region and Profile* subroutine with "Mean Filter" selected. Note the smoothing of the tritium image and tritium profile.

Figure 30: Front panel of the *Get Width from Profile* subroutine with smoothed profile as input. Front panel shows a measured width of 0.101 inches at a threshold of 3.4312.

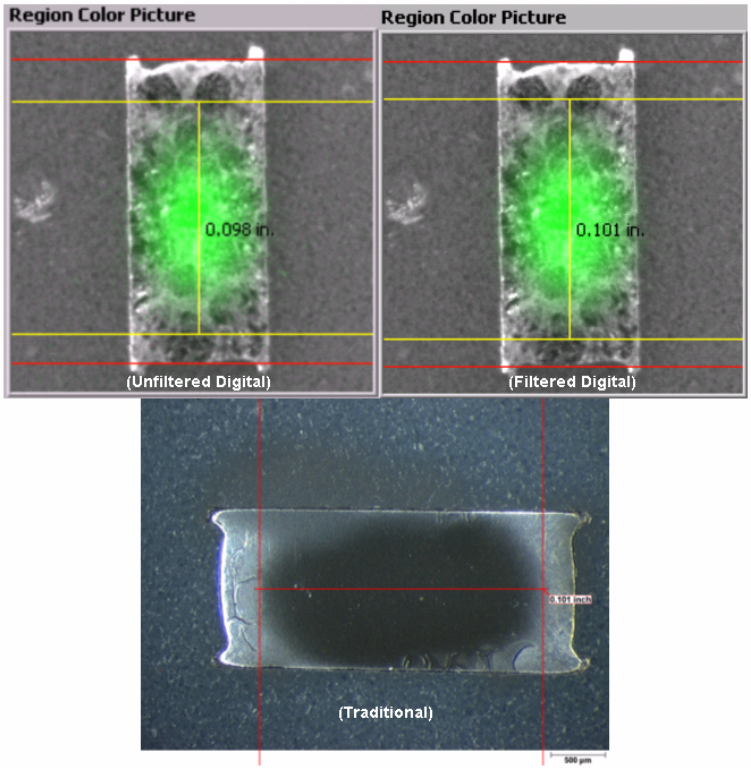

Figure 31: Comparison of the unfiltered digital (top left) and the filtered digital (top right) and traditional (bottom) results for the same sample.

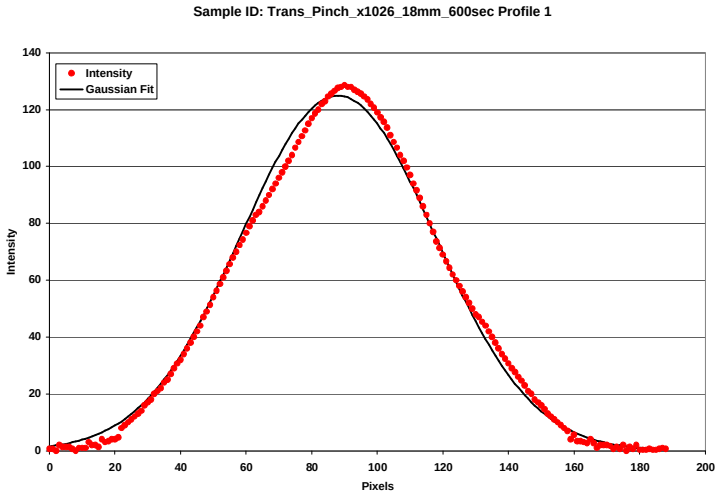

Figure 32: Profile intensity data compared against Gaussian distribution fit.

Comparison Study

To determine how well the two methods compared, a study was performed in which data was obtained using both methods on the same samples. Twenty-five samples, listed in Table 1, were evaluated using both techniques. Samples were chosen so that the overall population contained at least one of the following stainless steel alloys (21-6-9, 304L, and 316), and various sample geometries (longitudinal pinch weld, transverse pinch weld, girth weld, bulkhead weld, reclamation weld, fill bore, parent material, and end cap weld). In addition, the chosen samples ranged from very low expected tritium concentration to very high.

The results showed that the digital system provided "qualitative" results that demonstrated reasonable agreement with the traditional method on all samples. That is, the tritium image acquired from the digital method was similar to the image obtained with the traditional method, as shown in Figure 33.

The "quantitative" comparison consisted of measuring tritium penetration on samples using both methods. As can be expected with the comparison of any two measurement techniques, this task was not without challenges and issues. The primary difficulty with the comparison of any two measurement techniques is the availability of suitable "known" standards. Given such standards, the comparison between the measurement techniques is straight forward and easily quantifiable. However, in this case, suitable test standards do not exist. Therefore, it was assumed that the traditional method results are the "standard."

Several sources of variability with the measurement technique exist with both methods. For the traditional method, these sources include the variability in the application of the photo-emulsion coating, which can potentially spread contamination across the sample

Table 1: List of Samples in the Autoradiography Comparison Study.

	Sample ID	Reservoir Type	Material Type	Digital AutoRad Date	Traditional AutoRad Date	Sample Type
1	2M-281289	2M	21-6-9	1/31/2006	2/1/2006	Long. Pinch
2	1MK-5322	1M	21-6-9	2/9/2006	2/7/2006	Girth
3	1M-282026	1M	21-6-9	4/5/2006	1/25/2006	Girth
4	1X-20329	1X	304L	4/20/2006	2/15/2006	Bulkhead
5	LF7-K1083	LF7	304L	4/20/2006	4/20/2006	Reclam.
6	20041	1X	304L	4/26/2006	4/20/2006	Long. Pinch
7	X1026	1X	304L	4/26/2006	4/20/06, 5/10/06	Trans. Pinch
8	X0014	1X	304L	5/4/2006	4/20/2006	Long. Pinch
9	X1025	1X	304L	5/4/2006	4/20/2006	Long. Pinch
10	20962A	981A	304L	5/9/2006	5/10/2006	Girth
11	210040_B	1K	21-6-9	5/9/2006	5/10/2006	Fill bore
12	210040	1K	21-6-9	5/9/2006	5/10/2006	Reclam.
13	4002-6-1	3T	316	5/17/2006	5/22/2006	SS Sample
14	K1033-2-1	3T	316	5/17/2006	5/10/2006	SS Sample
15	3328	3T	316	5/17/2006	5/22/2006	Cap 2 PM
16	1K-303001	1K	21-6-9	5/30/2006	6/1/2006	Long. Pinch
17	1K-303052	1K	21-6-9	5/30/2006	6/1/2006	Long. Pinch
18	1M-303103	1M	21-6-9	6/6/2006	6/15/06, 6/20/06	Long. Pinch
19	1M-303103	1M	21-6-9	6/6/2006	6/15/06, 6/20/06	Girth
20	X0012	1X	304L	6/14/2006	6/21/2006	Long. Pinch
21	X1021	1X	304L	6/15/2006	6/21/2006	Long. Pinch
22	3328	3T	316	6/16/2006	5/22/06, 7/6/06	End Cap
23	X0011	1X	304L	6/19/2006	6/21/2006	Long. Pinch
24	K1008	3T	316	6/26/2006	6/22/2006	End Cap
25	K1033	3T	316	6/26/2006	5/16/06, 7/6/06	End Cap

surface, the variability in the exposure and development times, and in the visual subjectivity of the identification of the edge of the penetration. For the digital technique, the sources of variability include the exposure time, and the effect of "noise" level of the digital images. Other issues that impact the measurement comparison between the two inspection techniques include the elapsed time between the two inspections and the specific location of the measurement on the sample.

As mentioned above, the subjectivity in the identification of the edge location in the traditional method is a source of error. In the traditional method the evaluator must estimate the edge visually with no quantitative tools. Conversely, with the digital system it is possible to set the threshold value for the width measurement at a fixed percentage of the peak maximum or a fixed threshold value to obtain an objective unbiased measurement. A goal of the present study is to determine an estimate of the appropriate threshold value for penetration measurements.

The elapsed time is critical because tritium begins diffusing back out of the metal from the time the reservoir is unloaded. This process continues during sample preparation,

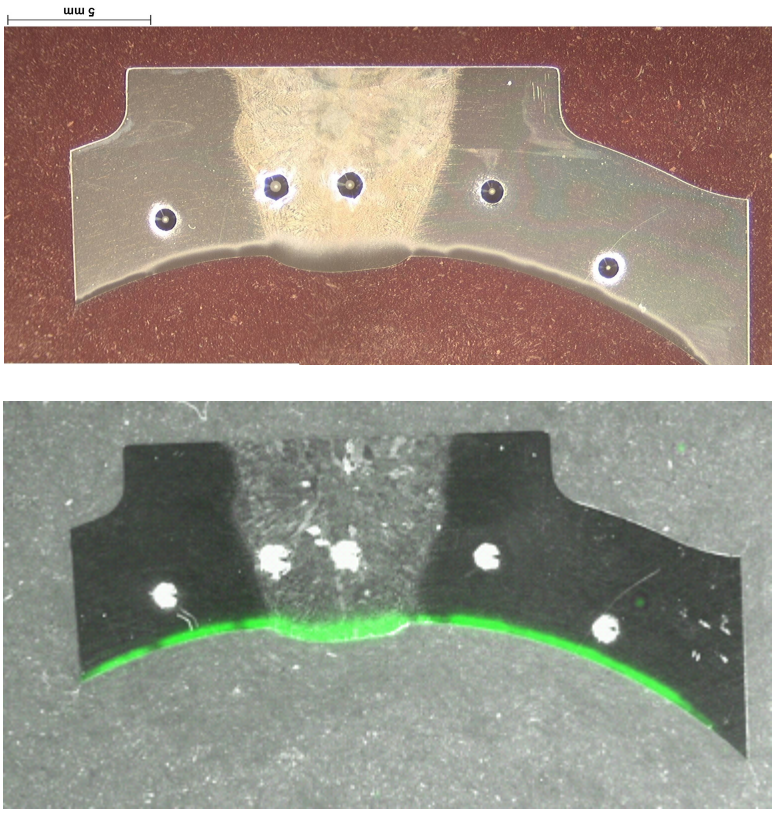

Figure 33: Typical "qualitative" comparison between traditional (top) and digital autoradiography (bottom) results (Sample 282026).

evaluation, and storage. Therefore, substantial time lags between the two methods will introduce errors in the comparison of the penetration measurement. This effect is illustrated in Figure 34, which depicts the traditional method results of two samples at two points in time. The top two photos (Sample X1026) show a change in measured penetration from 0.113 to 0.101 inches over the period of 20 days. The bottom two photos (Sample 20962A) show a change from 0.203 to 0.131 inches over a period of 246 days.

Another major factor of error in the comparison is the fact that the diffusion of tritium is not typically uniform and the measured result varies somewhat with the location of the measurement. Since the measurements were made by one author from the traditional results and by the other author from the digital results, some error is undoubtedly introduced by making the measurement at slightly different locations on the sample.

A further complicating factor is that the tritium concentration varies with each sample. The theoretical concentration depends on tritium pressure, storage temperature, time of storage, time between unloading and preparation of the metallographic mount, and other factors. The tritium concentration impacts the exposure time for both methods. For low concentration samples, the traditional method exposure time may be 2 days or longer to obtain an acceptable result. For the digital system, an exposure time of 3600 seconds

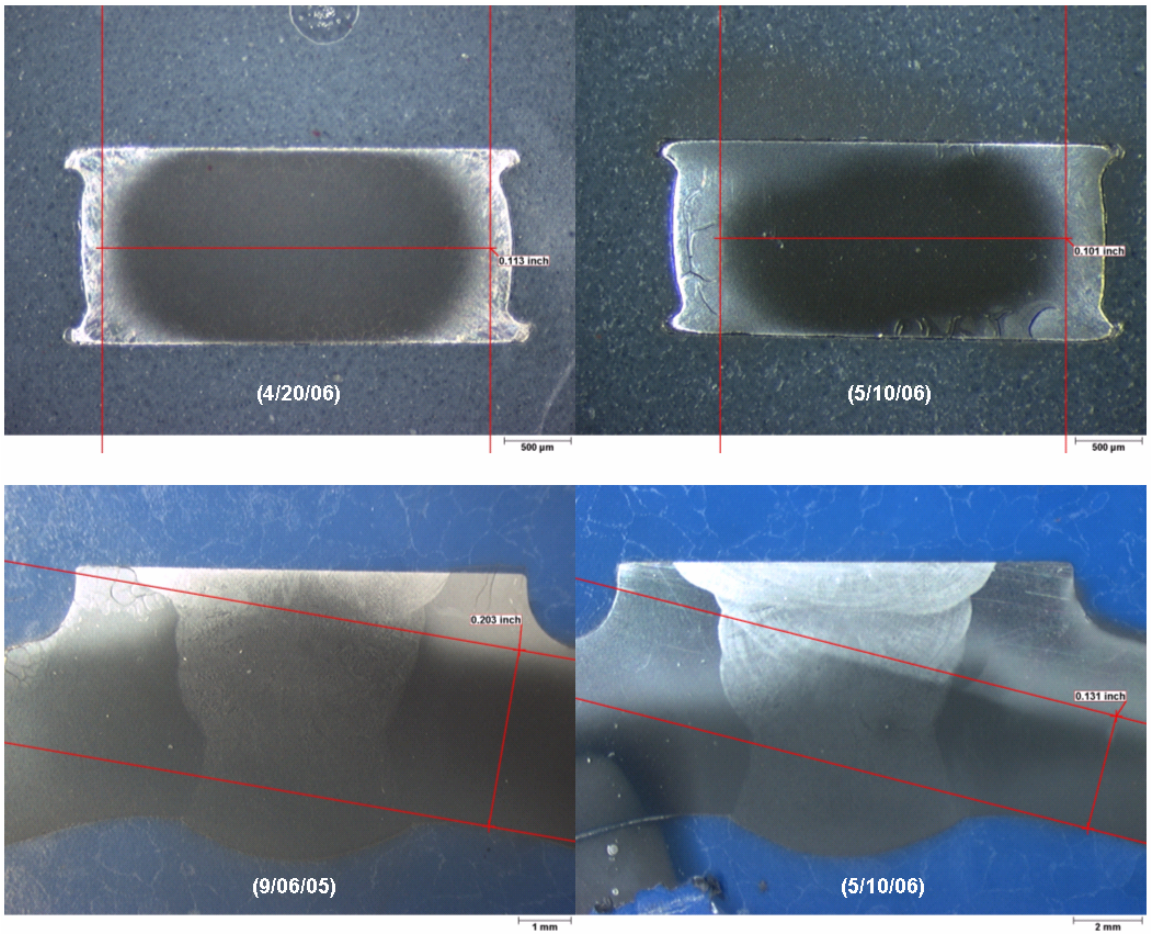

Figure 34: Effect of elapsed time on traditional results. Top: Transverse pinch weld (Type 1X, Sample ID X1026) on 4-20-2006 (left) and 5-10-2006 (right). Bottom: Girth weld (Type 981-A, Sample ID 20962A) on 9-6-2005 (left) and 5-10-2006 (right).

(1 hour) may be required rather than the typical exposures of 300 to 600 seconds. Longer exposures on both methods will tend to cause the measured penetration depth to appear larger. This issue is illustrated in Figure 35, which shows the Gaussian function fit to actual data taken on Sample X1026, a transverse pinch weld sample, at 300, 600, and 1200 seconds. As can be seen, if a constant threshold value is used to measure the penetration width, the measured width will generally increase with exposure time as shown.

Figure 36 shows the measurement of penetration depth on sample 3T-K1008 using the traditional method (top) and the result of using the traditional measurement tools on the digital color composite image (bottom). The digital system places a "scale bar" at the bottom of each image so that stand alone image processing software can be "calibrated" to allow measurements to be taken directly from the stored image. As can be seen, there is reasonable agreement between the two measurements (0.048 compared to 0.056 inches) using this technique.

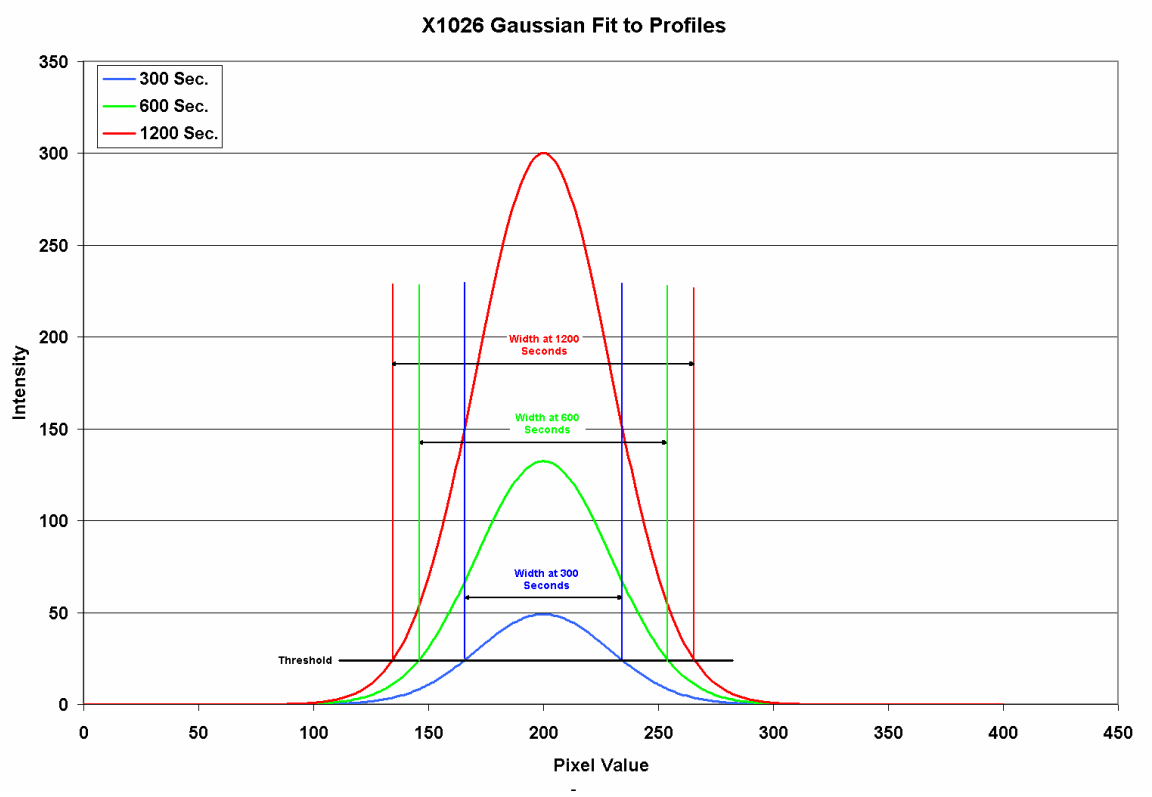

Figure 35: Effect of exposure time on the penetration depth (or width) measurement.

As stated previously, the digital imaging method allows for a more precise and less subjective penetration measurement. Manually setting the threshold value to just above the background noise level, the measured depth of tritium penetration was 0.066 inches, as seen in Figure 37.

This indicates an obvious discrepancy of 0.018 inches from the traditional measurement of 0.048 inches. It is difficult to assess the cause of this discrepancy. It could be due to inadequacies with the current method or could be associated with the exposure time and threshold used in the digital method. This discrepancy also illustrates the issue with making accurate penetration measurements directly from the image (Figure 36) without the benefit of the intensity distribution information.

Ideally, it would be advantageous to calibrate the digital system so that the image intensity could be correlated to a specific tritium concentration for a given exposure time and FOV. The traditional method measurement is predicated on the assumption that for 24 hour exposures the minimum density observable in the photo-emulsion is correlated to a tritium concentration of 0.1 part per million by weight (wppm) [3, 4]. If this 0.1 wppm level can be correlated to an intensity value, this value would be used for the threshold setting. Then as long as the selected exposure time resulted in an image where the

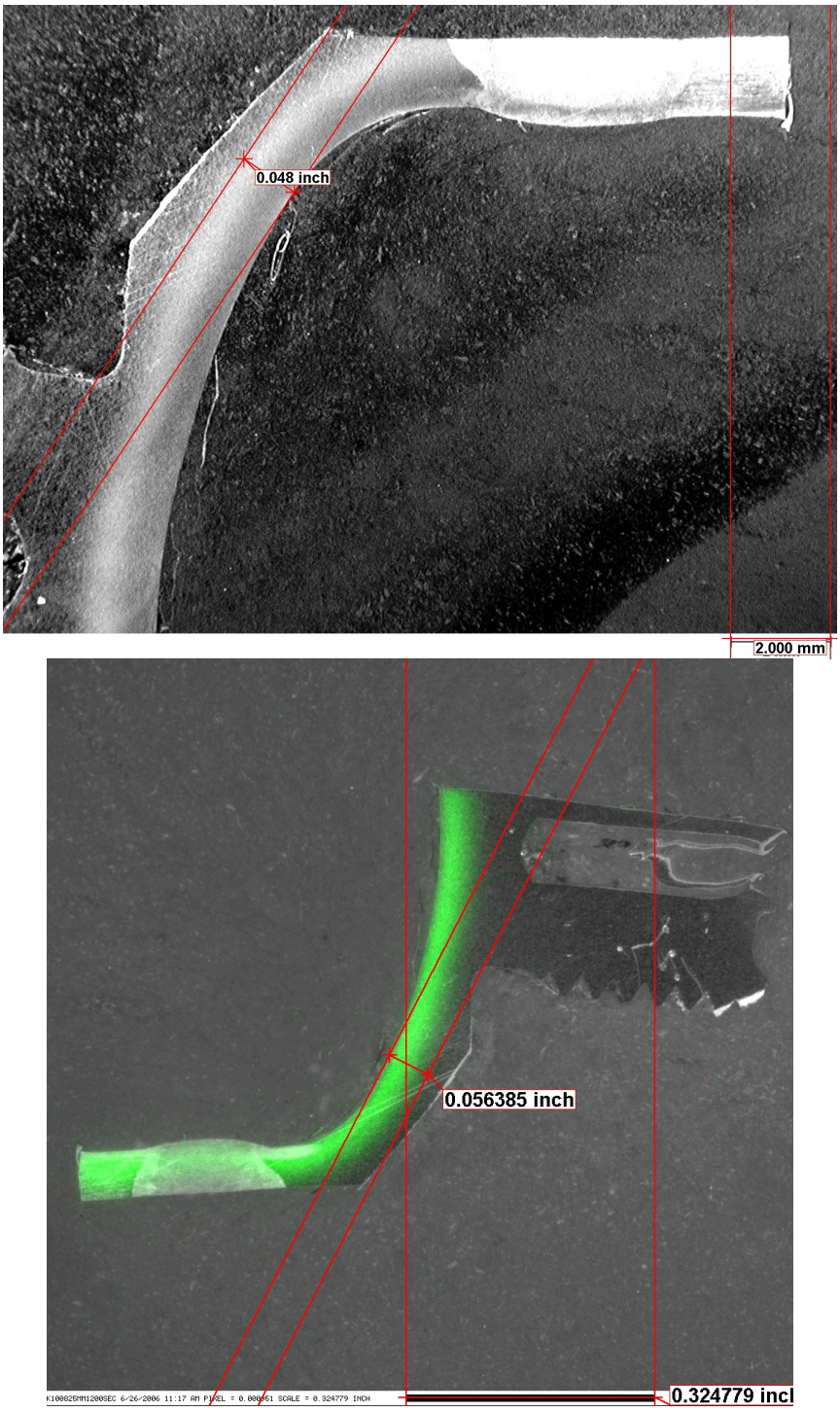

Figure 36: Top: Traditional measurement of sample 3T-K1008 showing penetration depth of 0.048 inches. Bottom: Traditional measurement tools used on digital color composite image of sample 3T-K1008 showing penetration depth of 0.056 inches.

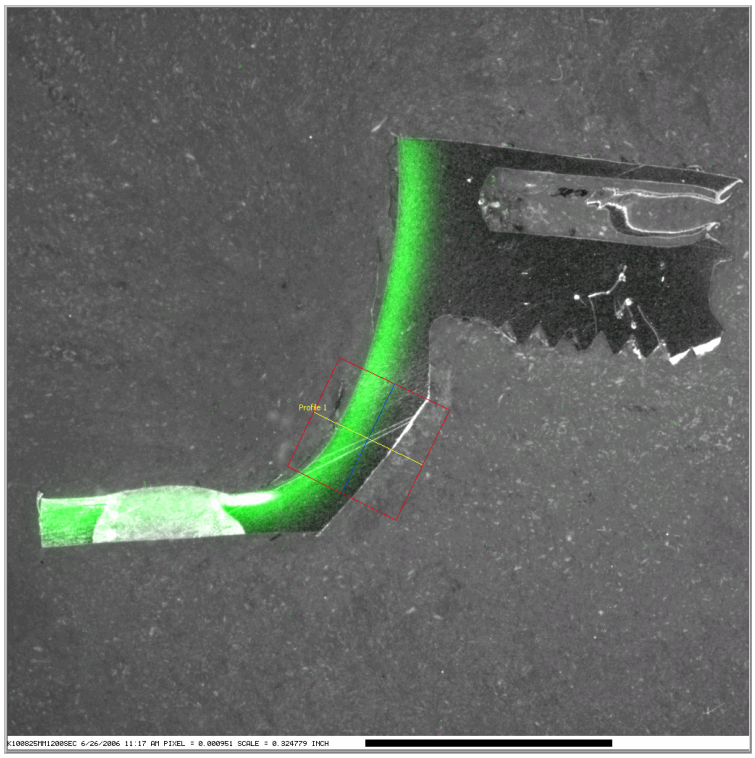

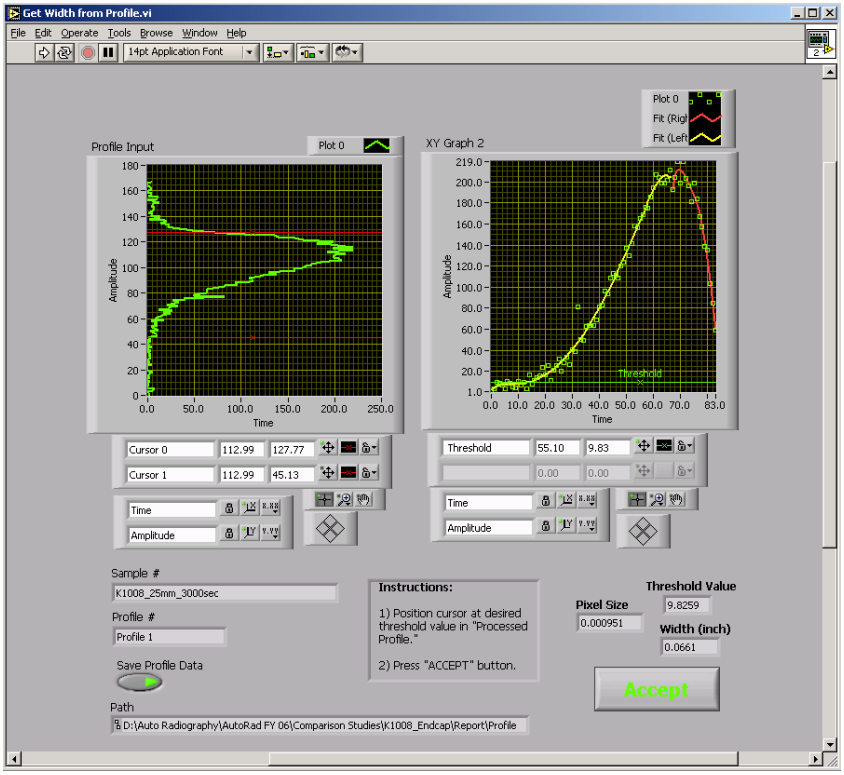

Figure 37: Measurement software result of sample 3T-K1008 showing penetration depth of 0.066 inches. Sample image with region and profile line (yellow) shown (top) and "Get Width from Profile" window showing threshold setting and measured width (bottom).

calculated 0.1 wppm threshold level was above the system noise level, the image would be considered acceptable.

In order to provide a rough correlation of CCD intensity to tritium concentration (C_T), the following methodology was applied. The "ACM Diff" code penetration values calculated at the 1 atomic part per million (appm) were available for a limited number of the samples in the study population. For comparison, 1 wppm is equivalent to about 55.8 appm. Therefore, the ACM Diff code penetration values are calculated at a level of 0.018 wppm, which is reasonably close to the accepted 0.1 wppm for penetration depth measurement referenced above. Two samples for which the traditional and digital results were in agreement with the ACM Diff code results were used to establish this correlation. In addition, empirical data relating the CCD intensity to the system FOV and exposure time were also used to derive a working model of the relationship between CCD intensity and tritium concentration. Figure 38 shows the empirical relationship of CCD intensity to system FOV under constant lighting conditions. The nonlinear relationship is due to the interplay between the intensity being directly proportional to the area per pixel and the reduction in solid angle subtended by the lens aperture as a function of working distance. The linearity of the CCD intensity with exposure time (T_{exp}) is demonstrated in Figure 39. Lastly, the CCD camera analog to digital converter has a gain factor (G_F) setting that allows signal multiplication by a factor of 1, 2, or 4. Using the information above, the working model (Eq. 2) of CCD intensity as a function of the FOV, C_T, T_{exp} and G_F is derived.

Eq. 2
$$I = [6.537 \times \ln(FOV) - 11.91] \times \left[\frac{T_{\exp}}{1000}\right] \times [C_T] \times \left[\frac{G_F}{4}\right]$$

The FOV is in units of mm, T_{exp} is in units of seconds, C_T is in units of appm, G_F is unitless. For example, the sample in Figure 37 (3T-K1008) had a 25 mm FOV, a 3000 second exposure time, and a gain factor of 4, which yields a CCD intensity of 27.4 at the 1 appm tritium level using (Eq. 2). When this sample is reanalyzed, as seen in Figure 40, using the calculated 1 appm CCD intensity as the threshold level, the measured penetration depth is 0.054 inches. This value is much closer to the traditional result of 0.048 inches and the result obtained by using the traditional measurement tools on the digital system image of 0.056 inches. To evaluate the efficacy of this method, the results are compared to the results obtained when the background noise level is used to establish the threshold for penetration depth to be measured.

The results using the background noise threshold method are listed in Table 2 and the tritium concentration threshold method results are listed in Table 3. In each table the results are sorted from the largest negative deviation (Δ) to the largest positive deviation. Deviation is defined here as the difference between the digital and traditional penetration values. For the background noise method, the deviation range is 0.058 inches (from -0.037 to +0.021 inches), the mean deviation is -2.35E-04 inches, and the standard deviation is 1.02E-02 inches. For the tritium threshold method, the deviation range is 0.035 inches (from -0.026 to +0.009 inches), the mean deviation is 1.67E-04 inches, and

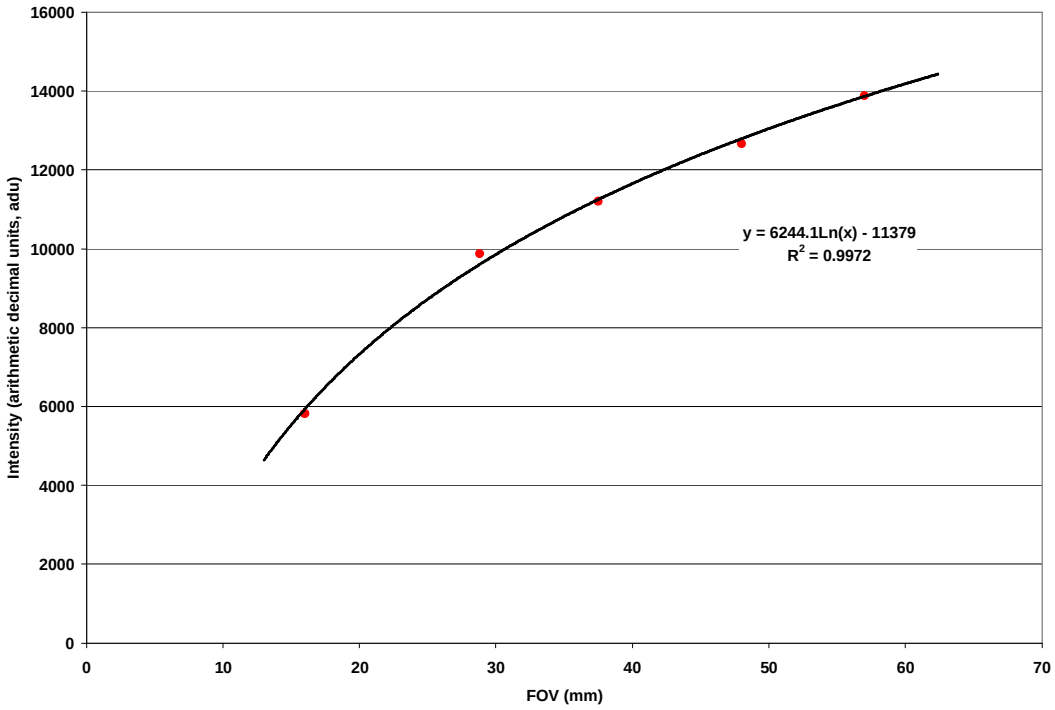

Figure 38: Empirical relationship of CCD intensity to system FOV under constant lighting conditions.

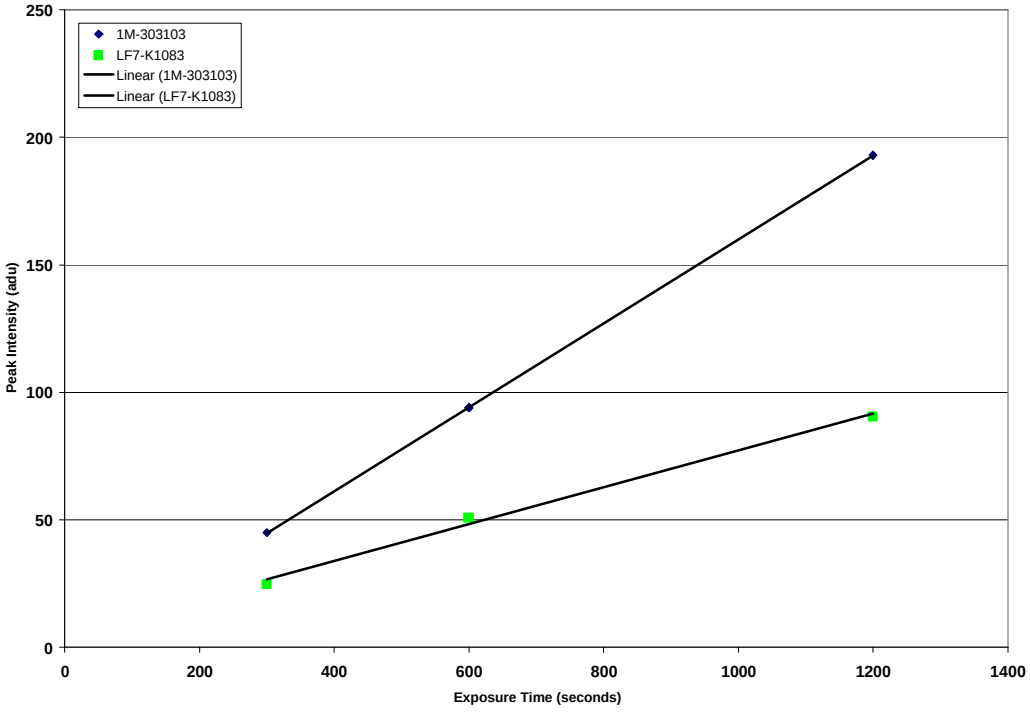

Figure 39: Empirical relationship of CCD intensity to exposure time showing linearity.

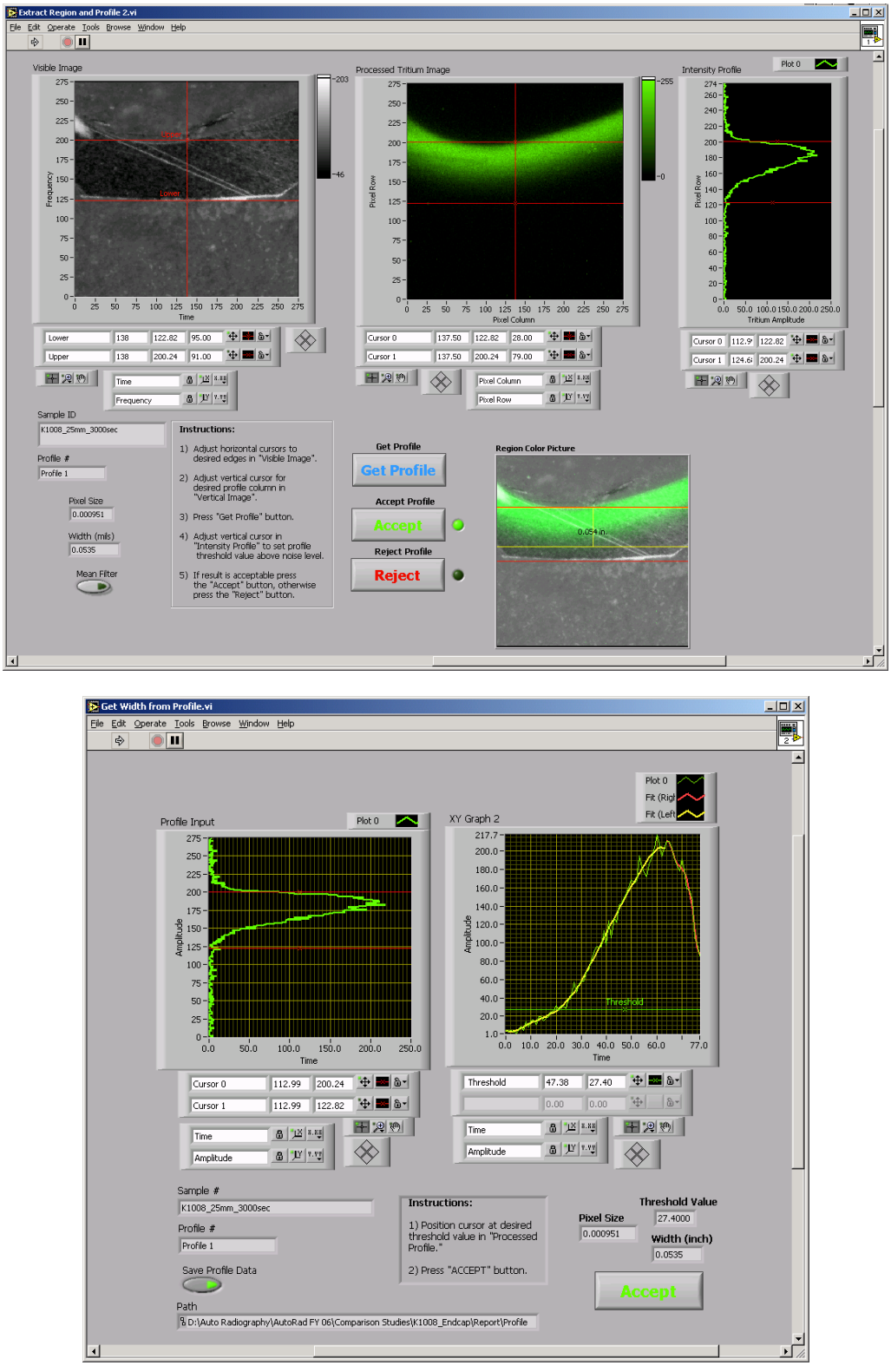

Figure 40: Measurement software results for sample 3T-K1008 showing a penetration depth of 0.054 inches with a 27.4 threshold (1 appm).

Table 2: Comparison results for "Background Noise Threshold Method".

Sample ID	Profile #	FOV (mm)	Gain Factor	T(exp) (sec.)	Peak	Threshold	Trad. (inch)	Digital (inch)	D (inch)
210040	1	18	4	300	14	2.9	0.064	0.027	-0.037
20962A	1	25	4	300	143	2.3	0.131	0.106	-0.025
210040_B	2	25	4	300	49	3.9	0.074	0.052	-0.022
X1026	1	18	4	300	70	5.7	0.101	0.084	-0.017
210040_B	1	25	4	300	63	3.5	0.075	0.065	-0.010
1X-20329	2	14	4	300	66	4.0	0.029	0.023	-0.006
210040_B	2	25	4	600	96	0.8	0.074	0.068	-0.006
X1026	1	18	4	600	142	3.5	0.101	0.097	-0.004
1M-282026	1	35	1	300	14	2.3	0.036	0.032	-0.004
210040	1	18	4	600	42	0.9	0.064	0.061	-0.003
1K-303001	1	18	4	600	121	na	0.025	0.022	-0.003
1K-303001	1	18	4	600	148	na	0.025	0.023	-0.002
LF7-K1083	2	14	4	600	50	1.0	0.022	0.020	-0.002
LF7-K1083	2	14	4	1200	91	1.1	0.022	0.021	-0.001
1K-303001	1	18	4	300	68	10.0	0.025	0.024	-0.001
LF7-K1083	1	14	4	300	52	3.2	0.021	0.020	-0.001
X1025	1	18	4	600	175	7.1	0.030	0.029	-0.001
X1025	1	18	4	300	94	8.1	0.030	0.029	-0.001
LF7-K1083	2	14	4	300	26	2.4	0.022	0.021	-0.001
K1033-2-1	1	18	4	600	32	2.5	0.050	0.049	-0.001
1M-282026	1	35	1	600	24	3.8	0.036	0.036	0.000
1X-20329	2	14	4	600	135	2.0	0.029	0.029	0.000
1MK-5322	1	25	1	600	7	3.0	0.010	0.010	0.000
LF7-K1083	1	14	4	1200	199	8.9	0.021	0.021	0.000
LF7-K1083	1	14	4	600	98	4.4	0.021	0.022	0.001
210040_B	1	25	4	600	101	1.0	0.075	0.076	0.001
1M-282026	3	35	1	300	15	3.1	0.016	0.017	0.001
1M-303103	2	25	4	600	91	7.4	0.026	0.027	0.001
1M-303103	2	25	4	300	48	6.3	0.026	0.027	0.001
1MK-5322	2	25	1	600	7.4	3.4	0.012	0.013	0.001
1X-20329	1	14	4	300	87	3.1	0.030	0.032	0.002
1M-303103	1	25	4	600	99	9.0	0.068	0.071	0.003
1M-282026	3	35	1	600	25	3.6	0.016	0.019	0.003
1M-282026	2	35	1	600	29	3.6	0.018	0.021	0.003
K1033-2-1	1	18	4	300	27	0.0	0.050	0.053	0.003
1M-282026	2	35	1	300	14	2.1	0.018	0.022	0.004
1M-303103	1	25	4	300	52	5.7	0.068	0.074	0.006
3328	1	25	1	1200	9	3.4	0.042	0.048	0.006
1M-303103	1	25	4	1200	174	5.2	0.068	0.075	0.007
K1008	1	25	4	1200	90	9.2	0.048	0.055	0.007
1X-20329	1	14	4	600	154	2.5	0.030	0.038	0.008
1M-303103	2	25	4	1200	185	8.3	0.026	0.035	0.009
X1026	1	18	4	1200	259	3.5	0.101	0.114	0.013
1MK-5322	2	25	1	1200	15	0.9	0.012	0.030	0.018
K1008	1	25	4	3000	219	9.8	0.048	0.066	0.018
1MK-5322	1	25	1	1200	11	1.1	0.010	0.031	0.021

Table 3: Comparison results for "Tritium Concentration (1 appm) Threshold Method".

Sample ID	Profile #	FOV (mm)	Gain Factor	T(exp) (sec.)	Peak	Threshold	Trad. (inch)	Digital (inch)	D (inch)
210040	1	18	4	600	45	4.2	0.064	0.038	-0.026
20962A	1	25	4	300	143	2.7	0.131	0.107	-0.024
210040	1	18	4	300	16	2.1	0.064	0.040	-0.024
210040_B	2	25	4	300	51	2.7	0.074	0.056	-0.018
210040_B	2	25	4	600	111	5.5	0.074	0.061	-0.013
210040_B	1	25	4	300	65	2.7	0.075	0.063	-0.013
210040_B	1	25	4	600	118	5.5	0.075	0.071	-0.004
K1033-2-1	1	18	4	600	32	4.2	0.050	0.046	-0.004
1X-20329	2	14	4	600	135	3.2	0.029	0.026	-0.003
LF7-K1083	2	14	4	1200	91	6.4	0.022	0.019	-0.003
X1026	1	18	4	600	142	4.2	0.101	0.099	-0.002
LF7-K1083	2	14	4	600	50	3.2	0.022	0.020	-0.002
LF7-K1083	2	14	4	300	26	1.6	0.022	0.021	-0.001
1K-303001	1	18	4	600	148	15.8	0.025	0.025	0.000
1M-282026	3	35	1	300	15	2.8	0.016	0.016	0.000
X1026	1	18	4	1200	259	8.4	0.101	0.102	0.001
3328	1	25	1	1200	9	2.7	0.042	0.043	0.001
K1033-2-1	1	18	4	300	27	2.1	0.050	0.051	0.001
1K-303001	1	18	4	300	68	7.6	0.025	0.026	0.001
LF7-K1083	1	14	4	1200	199	6.4	0.021	0.022	0.001
X1025	1	18	4	600	175	4.2	0.030	0.031	0.001
X1025	1	18	4	300	94	2.1	0.030	0.031	0.001
LF7-K1083	1	14	4	600	98	3.2	0.021	0.023	0.002
1M-303103	2	25	4	300	48	2.7	0.026	0.029	0.003
LF7-K1083	1	14	4	300	52	1.6	0.021	0.024	0.003
1M-303103	1	25	4	600	99	5.5	0.068	0.071	0.003
1MK-5322	1	25	1	600	7	1.4	0.010	0.013	0.003
1X-20329	1	14	4	300	87	1.6	0.030	0.034	0.004
K1008	1	25	4	1200	90	11.0	0.048	0.053	0.005
X1026	1	18	4	300	70	2.1	0.101	0.106	0.005
K1008	1	25	4	3000	219	27.4	0.048	0.054	0.006
1MK-5322	2	25	1	600	7.4	1.4	0.012	0.018	0.006
1M-303103	2	25	4	1200	185	11.0	0.026	0.032	0.006
1M-303103	1	25	4	300	52	2.7	0.068	0.074	0.006
1X-20329	2	14	4	300	66	1.6	0.029	0.036	0.007
1M-282026	2	35	1	600	29	1.7	0.018	0.025	0.007
1M-282026	2	35	1	300	14	1.1	0.018	0.025	0.007
1M-303103	1	25	4	1200	174	11.0	0.068	0.075	0.007
1X-20329	1	14	4	600	154	3.2	0.030	0.038	0.008
1M-282026	1	35	1	600	24	1.7	0.036	0.044	0.008
1M-282026	3	35	1	600	25	1.7	0.016	0.024	0.008
1M-303103	2	25	4	600	91	5.5	0.026	0.034	0.008
1MK-5322	2	25	1	1200	15	2.7	0.012	0.020	0.008
1MK-5322	1	25	1	1200	11	2.7	0.010	0.019	0.009
1M-282026	1	35	1	300	14	0.8	0.036	0.045	0.009

the standard deviation is 0.89E-02 inches. These statistics indicate that the tritium concentration method is the preferable method.

The results in Table 3 are summarized in Figure 41, which shows the frequency distribution of the absolute value of the deviation between the traditional and digital autoradiography results. It shows that the deviations for 24 out of 45 measurements are within ± 0.005 inches, and 39 out of 45 are within ± 0.010 inches. The distribution also appears to be bi-modal with a second mode near a deviation of 0.025 inches. An argument can be made that the lower mode is a normal distribution of deviations and the higher mode is due to a special cause which at this point remains unidentified.

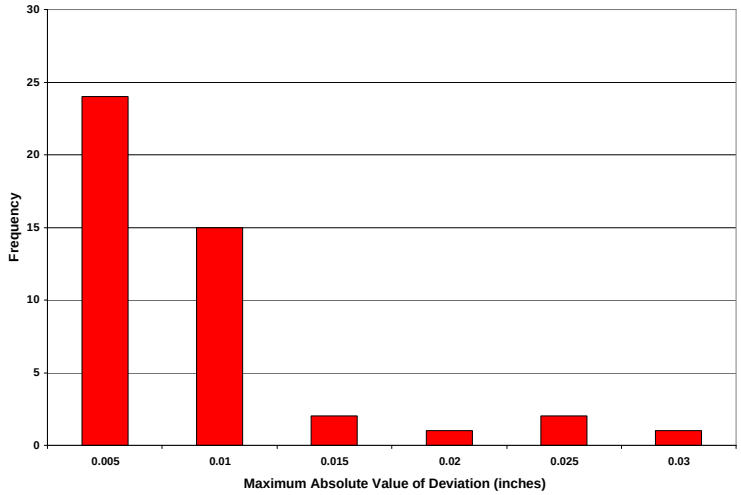

Figure 41: Summary of deviation using tritium concentration threshold method.

For the purposes of this comparison, the 24 measurements with deviations of ± 0.005 inches between the traditional and digital methods are considered to be essentially equivalent results. The deviations for these results are most likely due to slight differences in measurement location and subjectivity in the traditional measurement. Examples of two samples (1K-303001 and 1X-X1026) representing this case are provided below.

Figure 42 shows the traditional image and the digital color composite image for sample 1K-303001. The traditional measurement was 0.025 inches as shown. The measurement result of 0.025 inches from the digital system is shown in Figure 43. Figure 44 shows the traditional image and the digital color composite image for sample 1X-X1026. The traditional measurement was 0.101 inches as shown. The measurement result of 0.102 inches from the digital system is shown in Figure 45.

There were 15 measurements that had deviations between +0.006 and +0.009 inches. These results are conservative since the penetration depth is overestimated. For some of the results, the calculated thresholds were slightly below the noise level. Data points below the noise level are not considered reliable. In future work, if the 1 appm tritium

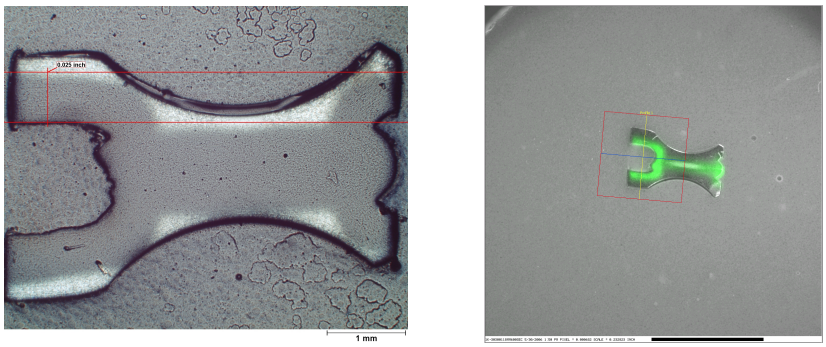

Figure 42: Traditional result and digital system result for Sample 1K-303001. (Note that digital image is inverted top to bottom with respect to traditional image.)

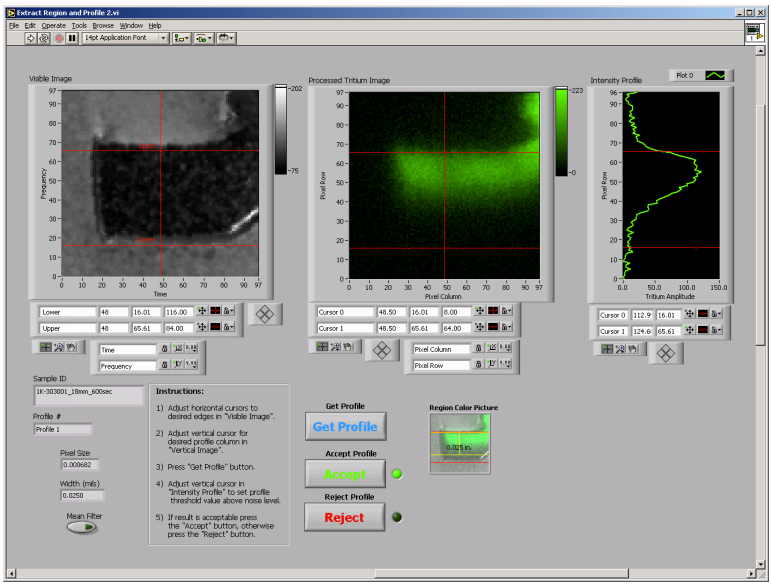

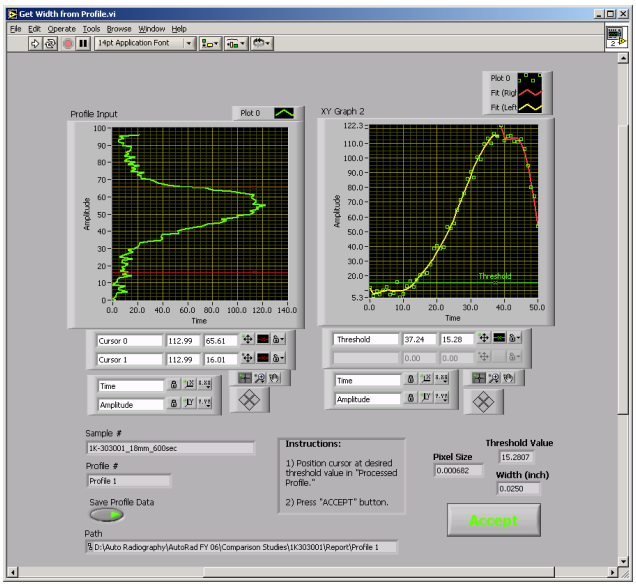

Figure 43: Measurement software result for sample 1K-303001 showing penetration of 0.025 inches, which agrees with the traditional result of 0.025 inches.

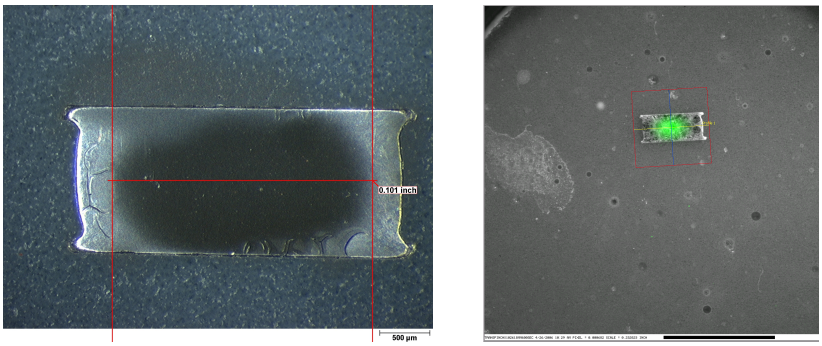

Figure 44: Traditional result and digital system result for Sample 1X-X1026.

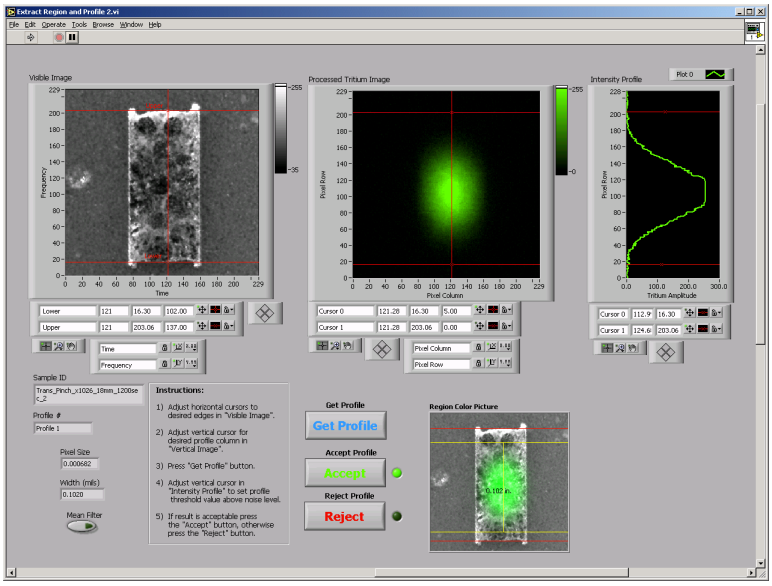

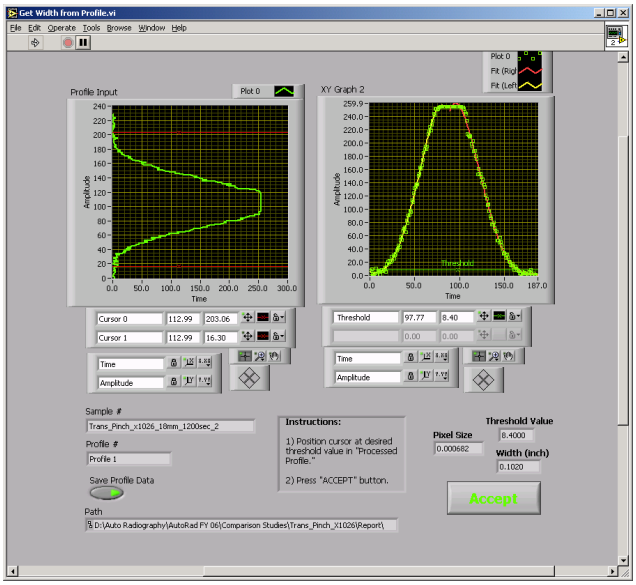

Figure 45: Measurement software result for sample 1X-X1026 showing penetration of 0.102 inches, which agrees well with the traditional result of 0.101 inches.

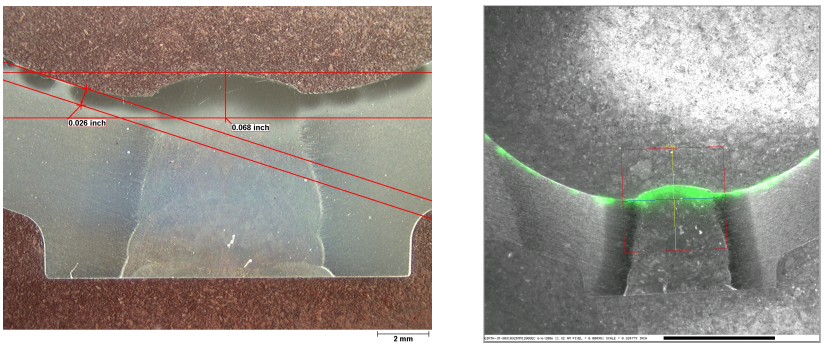

Figure 46: Traditional result and digital system result for Sample 1M-303103.

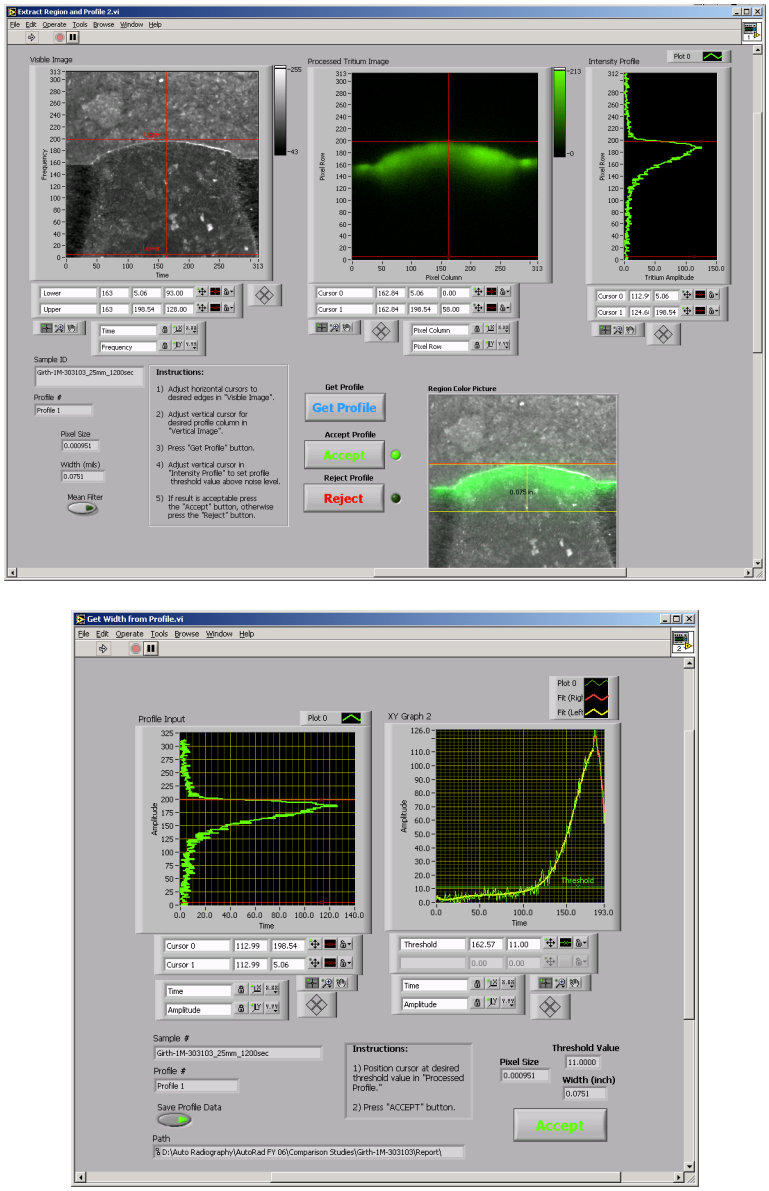

Figure 47: Measurement software result for sample 1M-303103 showing penetration of 0.075 inches compared to the traditional result of 0.068 inches.

concentration threshold level is below the background noise limit, the exposure time will be increased so that the 1 appm threshold is above the noise. The girth weld sample 1M-303103 is typical for this case and is shown in Figure 46. The measurement from the digital system of 0.075 inches is shown in Figure 47 and compares to the traditional value of 0.068 inches.

Lastly, there were six measurements that had deviations between -0.013 and -0.026 inches, which were associated with three samples (210040, 210040-B, and 20962A). It appears from the frequency distribution of the deviations (Figure 41) that these results are not part of the normally distributed deviation and may be attributed to a special cause. Two (-0.026 and -0.024 inches) of the six anomalous deviations in Table 3 are associated with sample 210040 (300 and 600 second exposures). We will review the 600 second exposure which accounts for the larger magnitude error below. Figure 48 shows a comparison of the traditional image and the digital color composite image for sample 1K-210040. The traditional measurement was 0.064 inches as shown. The measurement result of 0.038 inches from the digital system is shown in Figure 49.

One (-0.024 inches) of the six anomalous deviations in Table 3 is associated with sample 20962A. Figure 50 shows the traditional image and the digital color composite image. The traditional measurement was 0.131 inches as shown. The measurement result of 0.107 inches from the digital system is shown in Figure 51.

Three (-0.018, -0.013, and -0.013) of the six anomalous deviations in Table 3 are associated with sample 210040_B. The deviations on the 300 second exposures may be at least partially explained by the fact that the threshold value of 2.7 was below the estimated background noise level of 3.5 to 4.0 and consequently the measurements are not reliable. We will evaluate the deviation on the 600 second exposures. The traditional and digital images are shown in Figure 52. The traditional measurement was 0.075 inches for profile 1 and 0.074 inches on profile 2. The digital measurement result of 0.071 inches for profile 1 is shown in Figure 53. The digital measurement result of 0.061 inches for profile 2 is shown in Figure 54. The deviation for profile 1 was -0.004 inch and the deviation for profile 2 was -0.013 inch deviation. Since both are taken from the same digital image, it seems unlikely that measurement technique would work well in one instance and poorly in other. In this case, the reason for the deviation may be in the evaluation of the traditional results.

In general the comparison study has shown good agreement between the two methods both qualitatively and quantitatively for the majority of measurements. The larger deviations discussed above seem be due to a special cause. The three samples that had the large deviations were samples that had a large time lag between the traditional and digital methods. Consequently, after the digital technique was performed the traditional autoradiography technique was redone to provide a more recent traditional measurement. It is possible that these samples developed a thin oxide layer on the surface which would tend to attenuate the 18 keV beta particles prior to reaching the scintillator. This would cause the digital system to underestimate the penetration depth. If the samples were then

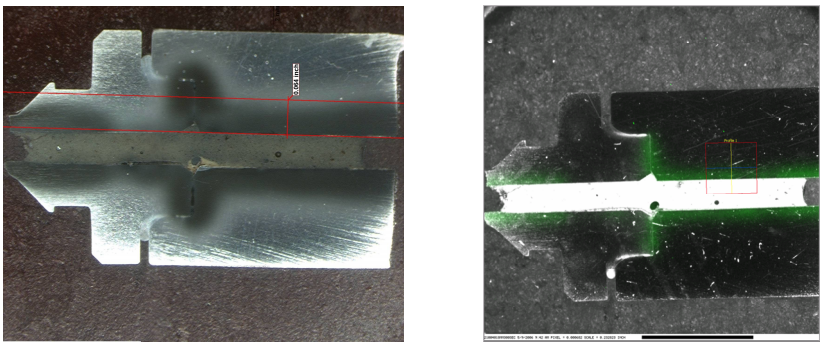

Figure 48: Traditional result and digital system result for Sample 1K-210040.

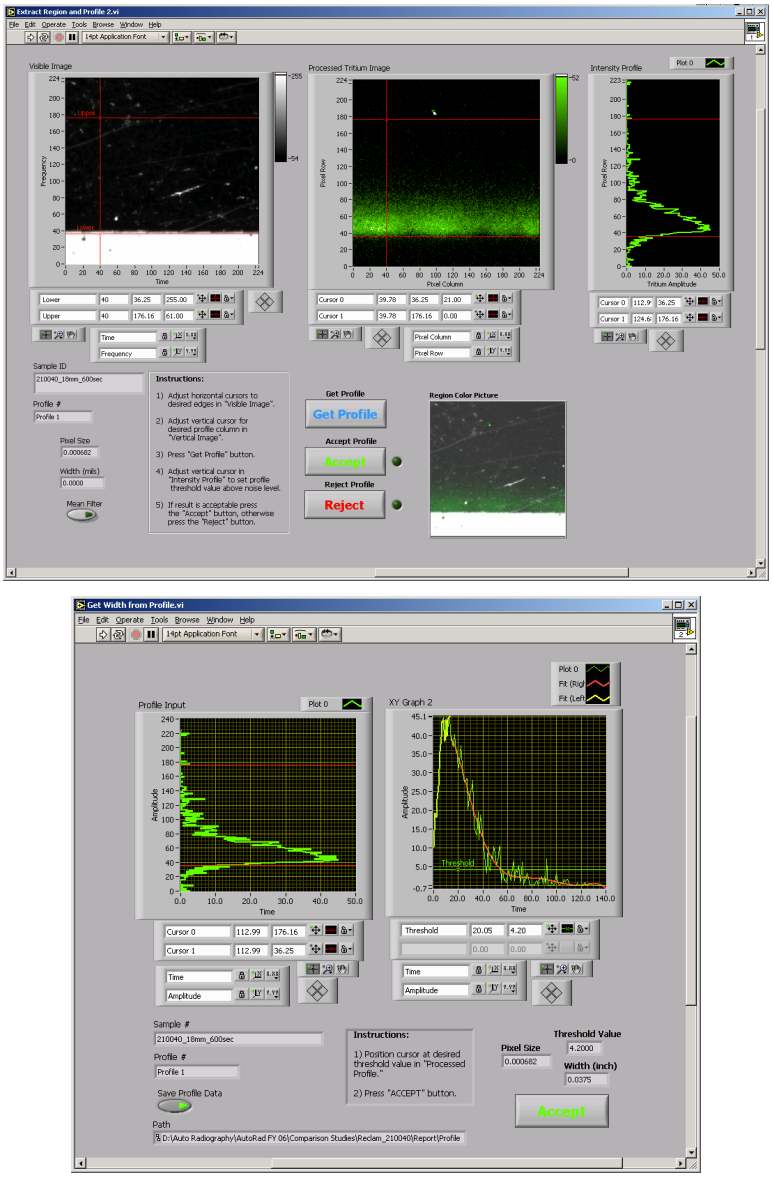

Figure 49: Measurement software result for sample 1K-210040 showing penetration of 0.038 inches compared to the traditional result of 0.064 inches.

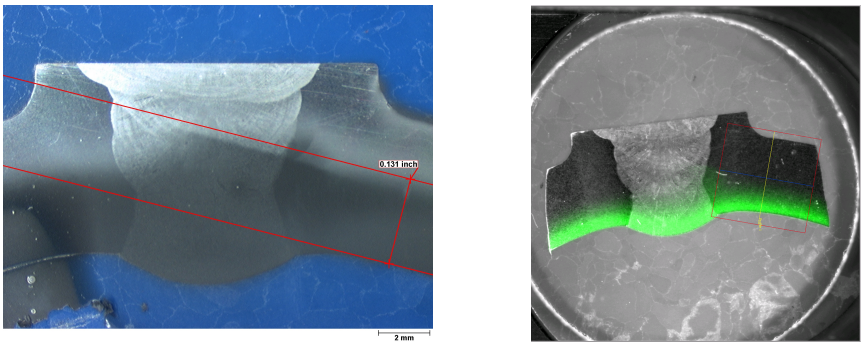

Figure 50: Traditional result and digital system result for Sample 20962A.

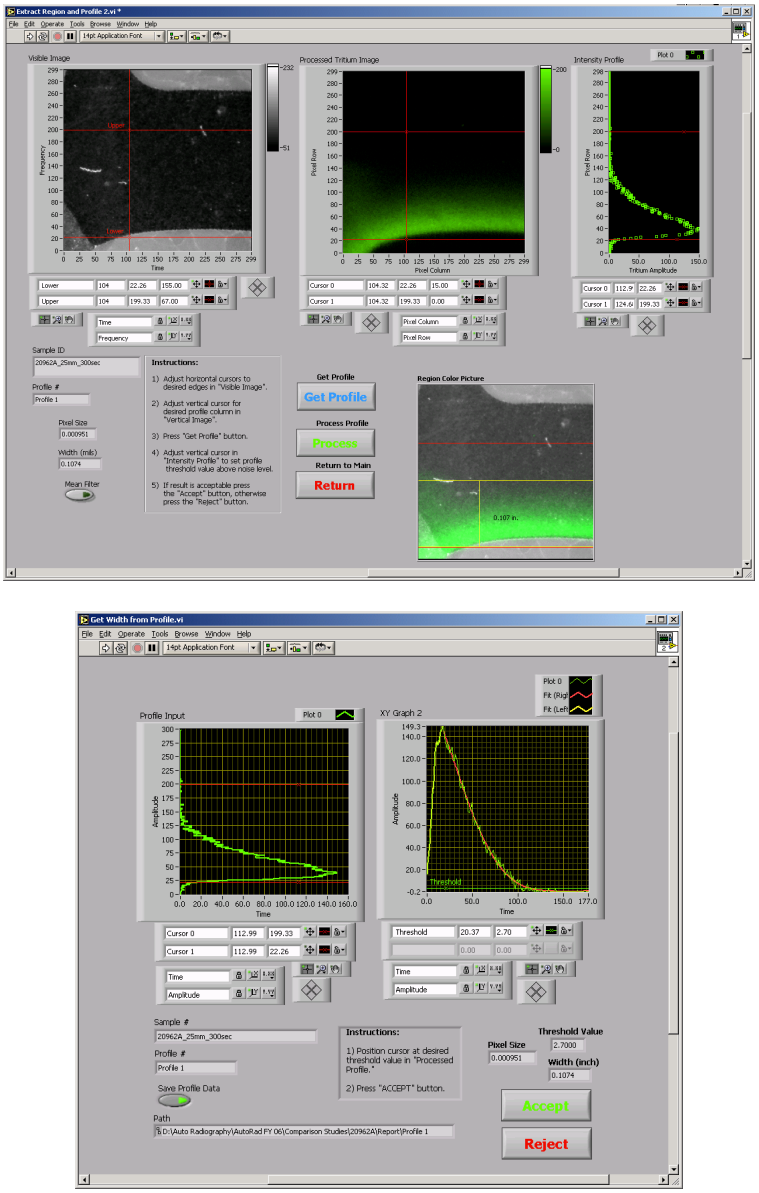

Figure 51: Measurement software result for Sample 20962A showing penetration of 0.107 inches compared to the traditional result of 0.131 inches.

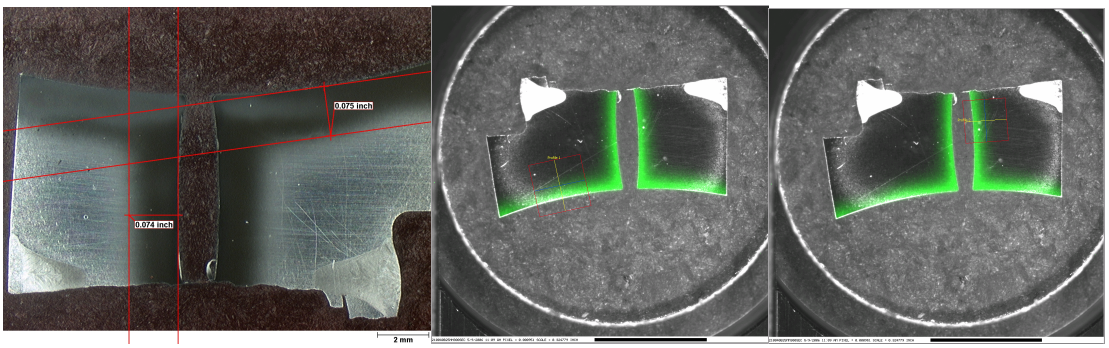

Figure 52: Traditional result and digital system results for Sample 210040_B.

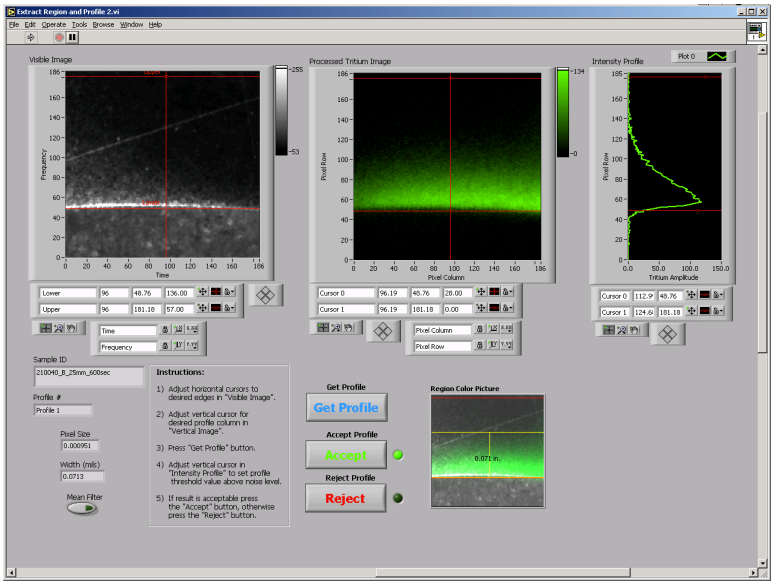

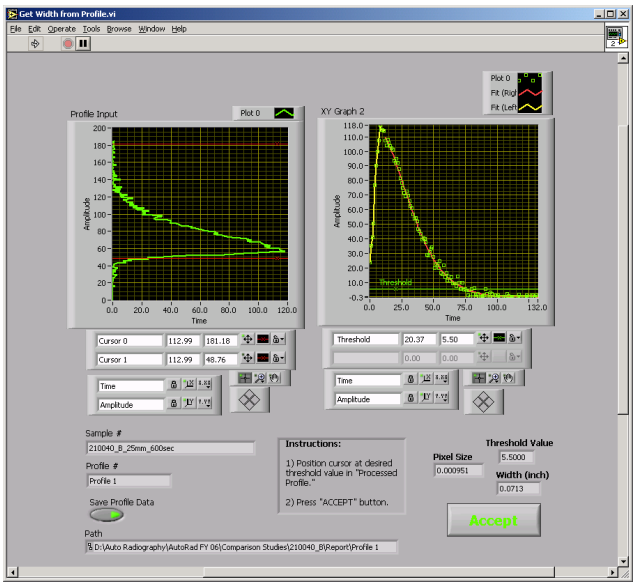

Figure 53: Measurement software result for Profile 1 of Sample 210040_B showing penetration of 0.071 inches compared to the traditional result of 0.075 inches.

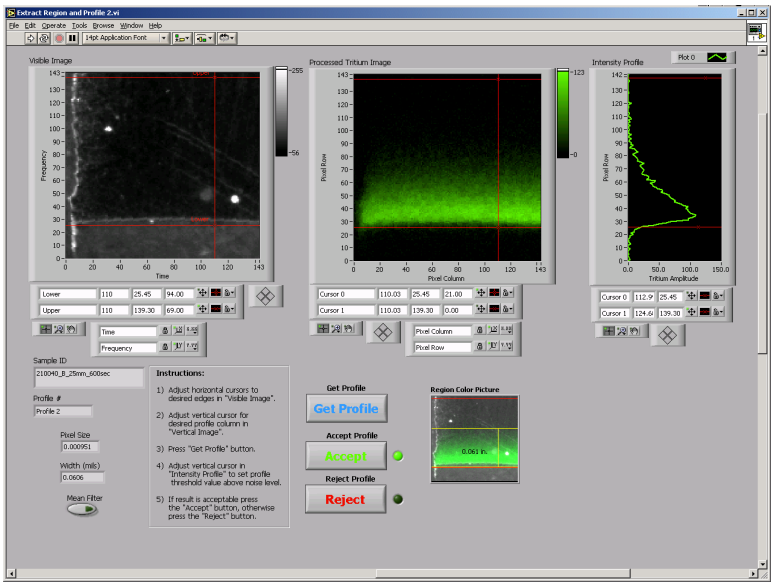

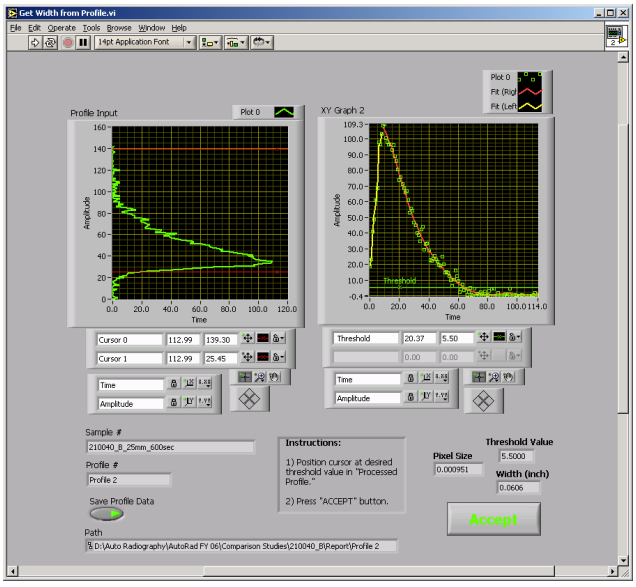

Figure 54: Measurement software result for Profile 2 of Sample 210040_B showing penetration of 0.061 inches compared to the traditional result of 0.074 inches.

polished or the surface cleaned prior to the application of the photo-emulsion for the second traditional autoradiography procedure, then this oxide coating was removed or perhaps fresh metal (with higher tritium concentration) was exposed. This would account for a larger tritium penetration measurement in the traditional method.

Conclusions

This report fulfills the FY 2006 Enhanced Surveillance Campaign Level 3 milestone for Task TSR 11.1 as defined in the execution plan [1, 2]. The purpose of this task is to reduce the cycle time necessary to complete analytical evaluations required for surveillance of reservoirs. The development of the digital autoradiography system supports this task. The digital autoradiography system is currently operational and ready for implementation in reservoir surveillance performed in the Materials Test Facility at SRS. SRS requests design agency (LANL and SNL) concurrence for the implementation of this system and on the establishment, in conjunction with SRNL, of the implementation requirements for this system.

This report has described the methodology of both the traditional and digital autoradiography techniques. A description of the digital imaging system design and evolution has also been provided. The custom software for image acquisition, processing, and penetration measurement has been documented. The method for system calibration for both dimensional measurement and for tritium concentration was also included in this report. Lastly, a comparison of the techniques on actual surveillance samples was provided.

The general conclusion from the comparison study is that the digital autoradiography technique produces similar results as the traditional autoradiography technique both qualitatively and quantitatively. Most quantitative measurements were basically equivalent between the techniques. However, the digital method can produce these images in 5 to 10 minutes of exposure, whereas the traditional method requires 24 hours or more.

The traditional method requires chemical processing, which can be eliminated with the adoption of the digital system. The Kodak NTB photo-emulsion used in the traditional technique requires refrigeration and has a limited (6 months) shelf life. A four ounce bottle costs over $800. In contrast, the digital method requires no chemical processing and the only consumable item is the scintillator screen. This item is commercially available from Kodak at the cost of about $200 for an 8 x 10 inch sheet. Less than ½ sheet has been consumed in two years of development work.

The traditional method requires more stringent sample preparation than the digital method. Any gaps between the sample and the mounting media are unacceptable because liquid can leach into and out of these gaps affecting the coating of the liquid photo-emulsion. This is not a concern with the digital method.

The traditional method results in saturation of the photographic emulsion and provides little information regarding the gradient of tritium concentration. The digital system has a linear response to tritium concentration so the gradient information is preserved.

Because the exposed emulsion is developed directly on the sample in the traditional method, the sample can be examined with optical and scanning electron microscopes at

any desired magnification. The digital method is limited to the FOV of the camera, which currently is in the 14 to 60 mm range. However, the corresponding pixel size ranges from approximately 0.0005 inches to 0.0024 inches, which is sufficient for the type of measurements being made on these samples.

There is typically more noise in the digital system due to the relatively short exposure time and the poor light collection efficiency of a lens compared to the efficiency of the photo-emulsion that is in direct contact with the sample. Even with the higher noise level, the needed measurements can still be made, especially if noise reduction image processing techniques are employed. Future work in this area could include the replacement of the off-the-shelf f/2.8 lens with a custom designed lens with greater light collection efficiency. For example, we could have two separate instruments each with a large aperture (f/1.0 to f1.2) fixed focal length lens. Based on the work here, one system with a fixed 35 mm FOV and one system with a 14 mm (or less) FOV. Other possibilities would be to replace the lens altogether in favor of a direct coupling between the sample and the CCD chip with a fiber optic coupler, or to employ an intensified CCD camera. All these methods could be used to reduce noise and or exposure time beyond what has already been achieved.

Based on the availability of funding, a more robust calibration of the CCD intensity as a function of tritium concentration could be beneficial. Samples of various concentrations of tritium would be inspected with the digital autoradiography system and the traditional technique and compared to the chemically determined tritium concentration. This work would enhance the value and accuracy of the digital technique.

Acknowledgements

Metallography and traditional autoradiography of the samples in this report were performed in the Material Test Facility metallurgical laboratory by Brenda Bordon, Josie Fraley, Pam Morgan, Sandra Stallings, Chiquita Johnson, and Lin Thacker.

References

1. WSRC-RP-2004-00743, FY2005-FY2010 Execution Plan, Enhanced Surveillance Campaign, Savannah River Site, E.J. Majzlik, Jr., November 15, 2004.

2. WSRC-RP-2006-00654, FY2006-FY2011 Execution Plan, Enhanced Surveillance Campaign, Savannah River Site, E.J. Majzlik, Jr., June 15, 2006.

3. J. D. Braun, G. L. Downs, and G. W. Powell, “An Autoradiographic Investigation of Tritium in 304L Stainless Steel,” Metallography (1971), pp. 231-242.

4. MD-10356, Issue 1, “General Operating Manual for SW Building Metallurgical Facilities,” September 12, 1991.

Distribution

E. R. Cochran, DOE, NNSA
R. Kumar, DOE, NNSA
S. H. Zaidi, DOE, NNSA
D. G. Williams, DOE, NNSA
B. L. Bulfinch, NNSA-SR, 235-H
T. G. Zocco, LANL
J. R. Carnes, ESA-GTS, MS C934, LANL
L. Najera, ESA-GTS, MS C934, LANL
R. Buley, ESA-GTS, MS C934, LANL
D. A. Lohmeier, ESA-GTS, MS C934, LANL
B. A. Meyer, ESA-GTS, MS C934, LANL
K. J. Chilcoat, ESA-GTS, MS C934, LANL
S. L. Hingorani, MS 0427, SNL/NM
J. W. Braithwaite, MS 0889, SNL/NM
R. J. Salzbrenner, MS 0885, SNL/NM
C. H. Cadden, Dept.08243, MS9108, SNL/CA
B. D. Oden, Dept.08243, MS9108, SNL/CA
C. W. Pretzel, Dept.08243, MS9108, SNL/CA
D. F. Cowgill, Dept.08243, MS9108, SNL/CA
D. K. Balch, Dept.08243, MS9108, SNL/CA
B. P. Somerday, MS9402, SNL/CA
L. J. Terminello, LLNL
A. J. Schwartz, LLNL
W. McLean, LLNL
B. Balazs, LLNL
S. A. Wood, DOE, NNSA, Pantex
B. D. Faubion, Pantex
P. L. Gorman, DOE, NNSA, ORO
R. Bonner, MS 8207, Y-12
R. Hayes, KCP
J. Engle, KCP
S. L. West, 773-A
M. H. Tosten, 773-A
G. K. Chapman, 773-A
P. S. Lam, 773-41A
A. J. Duncan, 773-A
P. S. Korinko, 773-A
E. A. Clark, 773-A
D. L. Hayes, 235-H
T. A. Foster, 235-H
B. D. Smith, 235-H
D. K. Utley, 235-H
S. L. Murphy, 249-H
K. G. Aylward, 235-H
J. P. Veldman, 773-A
L. M. Papouchado, 773-A
P. F. Cloessner, 773-A
A. F. Riechman, 773-A
S. B. Wyrick, 773-A
E. J. Majzlik, Jr., 773-A
E. G. Caveness, 773-A
D. L. Fish, 773-A
T. J. Warren, 773-A
R. T. Walters, 773-A
H. H. King, 234-H
C. S. Kestin, 234-H
M. B. White, 234-H
J. S. Holder, 999-2W
B. J. Cross, 730-2B
W. D. Rhodes, 999-2W
N. C. Iyer, 773-41A
M. E. Dupont, 773-41A
M. J. Morgan, 773-A
K. J. Imrich, 773-A
D. J. Green, 773-A
R. A. Haggard, 730-A
J. V. Cordaro, 723-A
W. D. Thompson, 723-A
K. M. Gibbs, 781-A
T. R. Smail, 781-A
B. Meers, 781-A
K. H. Subramanian, 773-A
R. L. Sindelar, 773-41A
E. G. Estochen, 773-A
Records, 773-52A